

Article

A Google Earth Engine-Based Framework to Identify Patterns and Drivers of Mariculture Dynamics in An Intensive Aquaculture Bay in China

Peng Wang¹, Jian Wang¹, Xiaoxiang Liu¹ and Jinliang Huang^{1,2,*}

¹ Coastal and Ocean Management Institute, College of the Environment and Ecology, Xiamen University, Xiamen 361102, China

² Fujian Key Laboratory of Coastal Pollution Prevention and Control, Xiamen University, Xiamen 361102, China

* Correspondence: jlh Huang@xmu.edu.cn ; Tel.: +86-13959290626

Abstract: Although mariculture contributes significantly to regional/local economic development, it also promotes environmental degradation. Therefore, it is essential to understand mariculture dynamics before taking adaptive measures to deal with it. In the present study, a framework that integrates the Google Earth Engine (GEE) based methods and GeoDetector software was developed to identify patterns and drivers of mariculture dynamics. This framework was then applied to Zhao'an Bay, which is an intensive aquaculture bay in Coastal China, based on Landsat 8 OLI (2013–2022) and Sentinel-2 (December 2015–May 2022) data. The results show that the GEE-based method produces acceptable classification accuracy. The overall accuracy values for the interpretation are >85%, where the kappa coefficients are >0.9 for all years, excluding 2015 (0.83). Mariculture increased in the study area from 2013 to 2022, and this is characterised by distinct spatiotemporal variations. Cage mariculture is primarily concentrated around islands, whereas raft mariculture is dominant in bay areas, and pond and mudflat mariculture types are mostly in nearshore areas. The growth of mariculture in Zhao'an Bay is attributed to a combination of geographic and human factors. The initial area associated with mariculture in a grid significantly impacted the expansion of the raft, cage, and mudflat mariculture. The distance to an island, spatial proximity to similar types of mariculture and types of mariculture are the main drivers of change in mariculture. Human activities greatly contribute to the dynamics of mudflat mariculture; regulation regarding the clearing of waterways directly impacts the dynamics of mariculture. The present study demonstrates that the proposed framework facilitates the effective monitoring of the mariculture dynamics and identification of driving factors. These findings can be exploited for the local planning and management of mariculture in similar coastal bays.

Keywords: bay; mariculture; GEE; random forest; spatiotemporal dynamics; driving forces

Citation: Wang, P.; Wang, J.; Liu, X.; Huang, J. A Google Earth Engine-Based Framework to Identify Patterns and Drivers of Mariculture Dynamics in An Intensive Aquaculture Bay in China. *Remote Sens.* **2023**, *15*, 763. <https://doi.org/10.3390/rs15030763>

Academic Editors: Wojciech Drzewiecki and Stanisław Lewiński

Received: 7 December 2022

Revised: 20 January 2023

Accepted: 24 January 2023

Published: 28 January 2023



Copyright: © 2023 by the authors. Licensee MDPI, Basel, Switzerland. This article is an open access article distributed under the terms and conditions of the Creative Commons Attribution (CC BY) license (<https://creativecommons.org/licenses/by/4.0/>).

1. Introduction

Ensuring the availability of food to an estimated 9.7 billion people in the world by 2030 is the second of the 17 Sustainable Development Goals (SDGs) of the United Nations [1]. Therefore, as a major food production sector, aquaculture has been characterised as a 'blue revolution', which can ease the pressure of the demand for food in the world. Excluding aquatic plants, fisheries and aquaculture production in the world increased by 41% from 2000 to 2019 [2]. Owing to their locations, coastal bays are attractive areas for mariculture [3,4]. However, even though mariculture in bays yields economic benefits to local communities, the associated ecosystems often experience tremendous stresses. The associated negative eco-environmental consequences include water pollution, the loss of coastal wetlands, and disease transmission [5–9]. Considering that China is the leading

country for aquaculture, understanding the dynamics of mariculture in coastal bays is of great significance [2].

Remote sensing is widely used in monitoring targets because of its extensive coverage and accessibility to areas that are otherwise difficult to reach [10,11]. However, existing studies focus on the extraction of a single type of aquaculture, which provided limited information on the spatiotemporal dynamics of aquacultures [12–16]. The extraction of information involving multiple aquaculture types is more useful for exploring changes in these areas [17]. Time-series optical imagery can effectively improve mapping accuracy [18,19]. The use of time-series remotely sensed data to extract all mariculture types is beneficial for understanding the spatiotemporal dynamics of these environments, which is the advantage of the Google Earth Engine (GEE) platform.

The emergence of the GEE cloud platform offers powerful means of monitoring targets using remotely sensed data, and this has been exploited in diverse sectors including agriculture, meteorology, water conservation, and e-commerce [20–23]. The MODIS, Landsat1-8, and Sentinel-1,2 imagery is commonly used to provide land use, vegetation, temperature, and other data for the GEE platform [24]. The GEE cloud platform involves data extraction techniques, such as threshold, support vector machine (SVM), and random forest [23,25,26]. For example, the performances of multiscale datasets were compared for the classification of rice cultivation using the random forest method on the GEE platform. Machine learning and cloud computing were employed based on Landsat 30 m and MODIS 250 m time-series data to develop three cropland products for South Asia using the GEE platform. The Landsat 8 OLI and Sentinel-2 images were pre-processed in the GEE platform using JavaScript, and the area covered by the Tuosu Lake was extracted by combining the NDWI (normalised difference water index), MNDWI (modified normalised difference water index), and SVM methods [26].

The extraction of aquaculture information based on remotely sensed images can be divided into two categories: cloud computing and local processing. In terms of local processing, aquaculture data have been extracted from remote sensing images using techniques such as deep learning, object-oriented automatic processing, and an improved U-Net with a PSE structure [12,27,28]. SAR images, such as those acquired by the Sentinel-1, were used to extract information on raft aquaculture using an improved statistical region merging (SRM) algorithm and a shape-constrained method [14,29]. Wang et al. [13] also extracted the coastal raft cultivation area that involves a heterogeneous water background via a thresholding object-based visually salient NDVI from imagery associated with a high spatial resolution. Concerning the GEE cloud processing, several studies on the extraction of aquaculture information from satellite data using this platform are available. A decision-tree classifier derived from the GEE cloud platform based on Landsat data, for example, was used to automatically identify ponds associated with major aquaculture [30]. A novel approach based on multisource spectral and texture features was proposed for the simultaneous mapping of inland and marine aquaculture areas [31]. The GEE cloud computing platform has also been used to extract aquaculture ponds on a national scale [15,16]. In addition, with the continuous development of relevant theories and algorithms of machine learning, compared with conventional classification methods, machine learning often produces better results in remotely sensed image classification [32–34]. For user convenience, the GEE platform integrates machine learning-related classification algorithms, including the random forest, decision tree, SVM, Naive Bayes and so on. It was found that the random forest method is the most frequently selected method in the GEE platform, exhibiting maximum overall accuracy compared to other classifiers [24]. As such, the random forest method in GEE has been widely used in the classification of remotely sensed images [35–37].

Owing to the mariculture sector, the marine environment has been altered in many areas. Spatiotemporal variations in aquaculture are controlled by confluence, geographic, and human factors [17,38]. Based on interviews with 67 aquaculture farmers, economic incentives account for the conversion from agriculture to aquaculture in the Indian

Sundarbans [39]. Additionally, analyses of factors controlling changes in aquacultures were mainly based on a regression model [17,38]. In contrast, GeoDetector is a robust and straightforward method to quantify the influences of driving factors and their interactions [40]. The methods employed can avoid interference due to subjective factors and yield more objective and accurate evaluation results [40]. This technique enables investigations of the combined effects of single and multiple factors as well as of the strength, direction, and linearity or nonlinearity of interactions in mariculture areas in a bay. The effectiveness, convenience, and validity of the GeoDetector software for the analysis of driving factors have been demonstrated in diverse fields, including agriculture, disease, climate, forests, water quality, wetlands, and urban sprawl [41–47].

Understanding the dynamics of mariculture development and the underlying driving forces is crucial for regulating mariculture development and improving water quality in the bay. In the present study, we conducted a thorough investigation of the mariculture dynamics in Zhao'an Bay, which is a typical mariculture bay on the southeast coast of China. Previous studies on aquaculture in Zhao'an Bay focused on its influence on the bay's water quality [48–51]. To our knowledge, there is no report about the remote sensing of mariculture dynamics in this bay. The objectives of the present study were: (1) to characterise the spatiotemporal dynamics of mariculture in the bay using the GEE online cloud platform, and (2) to identify potential drivers of changes in the environment. The findings of the present study can be used to improve maritime spatial planning and promote the sustainable development of mariculture locally.

2. Materials and Methodology

2.1. Study Area

Zhao'an Bay is on the southeast coast of Fujian Province and is surrounded by the Zhao'an, Dongshan, and Yunxiao counties. This bay, which covers an area of approximately 152.66 km², exhibits an N–S orientation and is characterised by a broad, shallow, and level seafloor (Figure 1). It represents an important environment for mariculture in Fujian Province. However, water quality in the bay has been deteriorating in recent years because of extensive mariculture. In 2021, this bay was listed among 14 with water quality worse than class V of the standard in China [52].

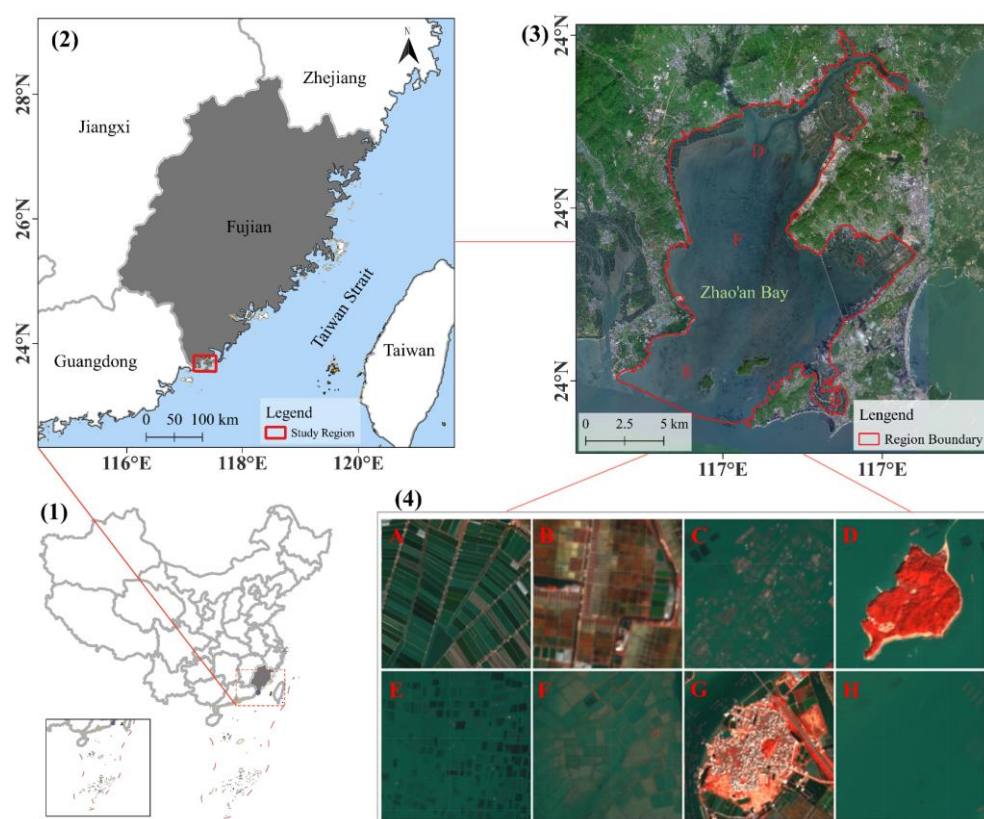


Figure 1. Maps showing the location of the study area and images of different mariculture types. (1)–(3) Location of study area at different scale; (4) Satellite image of different types of land cover. A: pond; B: salt pan; C: cage; D: vegetation cover; E: raft; F: mudflat; G: built-up land; H: seawater.

2.2. Methods

A flowchart of the methodology used in the present study is shown in Figure 2. The framework comprised the following components: (1) the extraction and classification of mariculture types, (2) an analysis of the expansion of mariculture, and (3) an analysis of forces controlling the mariculture dynamics.

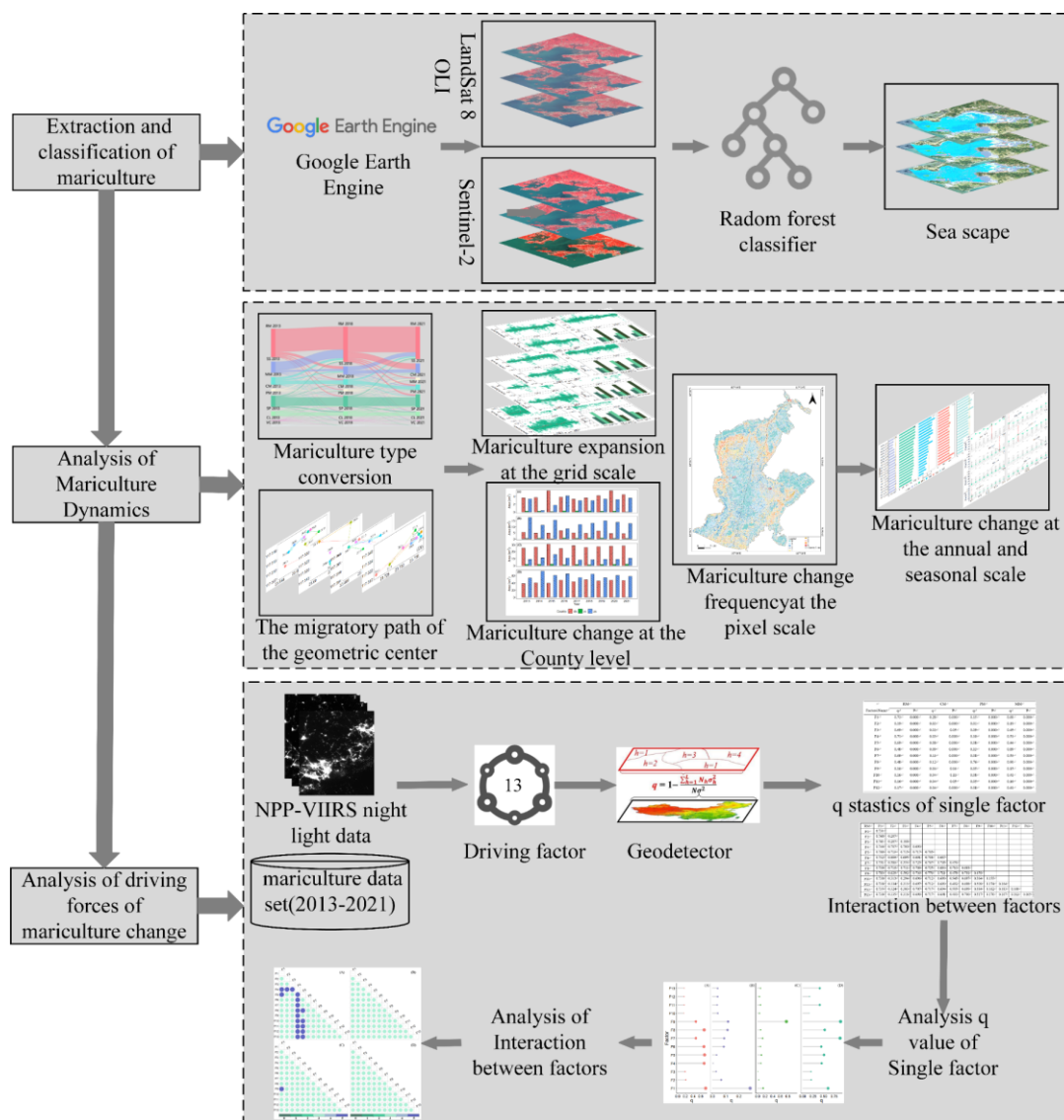


Figure 2. Flowchart of the methodology used in the present study.

2.2.1. Extraction and Classification of Mariculture

Sentinel-2 (January 2016–May 2022) and Landsat 8 OLI (2013–2021) data with a maximum cloud coverage of 10% per scene were processed in the present study using the GEE online platform. An annual average dataset was created based on multiple Landsat 8 OLI periods per year. Even though Sentinel-2 provides monthly imagery, June, July, and August are excluded because the cloud coverage during these months exceeds 10%. Annual and monthly spatial data on mariculture activity in the study area, which includes ponds, mudflats, rafts, cages, seawater, vegetation cover, salt pans, and construction land, were extracted using the random forest method through the GEE online platform. Remote sensing interpretation marks are shown in Table A1. The three steps followed to extract information on types of mariculture are displayed in Figure 3.

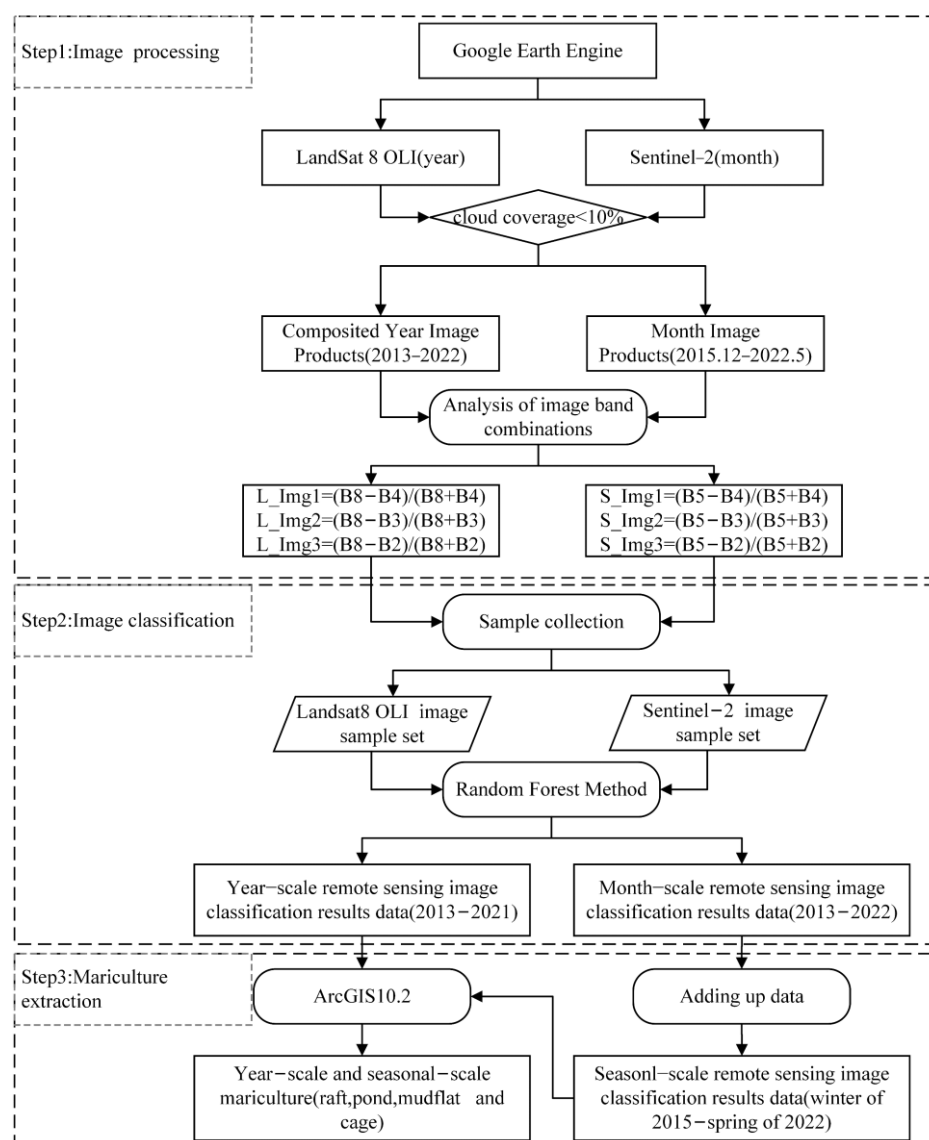


Figure 3. Flowchart for classification of types of mariculture.

Step 1: The GEE platform was used to filter images that involved <10% cloudiness, and this was followed by combining multiple appropriate images for each year into one image. The images were then tested using varying band combinations, and samples were selected based on the best composite images. Step 2: Land and marine cover data for the study area were then extracted from the images using the random forest method in the GEE platform. The overall accuracy and Kappa coefficient were calculated, and the associated images were downloaded. Step 3: The ArcGIS 10.2 software was then used to identify raft, pond, mudflat, and cage mariculture areas in the classification images. The bands of Landsat 8 used in this study include Band1–Band5 and Band7, with a spatial resolution of 30 m. The Sentinel-2 bands used include Band2–Band4 and Band8, with a spatial resolution of 10 m. The accuracy of the remote sensing image classification results in 2022 is verified in the field. The classification results of historical remote sensing images are verified by using an interactive interpretation method.

2.2.2. Analysis of Mariculture Dynamics

The dynamics of aquaculture over time in Zhao'an Bay were characterised based on the following aspects: (1) The overall change, which involves transitions between mariculture area types and the migration path of the geometric centre. (2) The spatial variation,

which reflects the administrative boundary (county), pixel-scale change frequency of mariculture and grid-scale dynamics of mariculture, including the amount, extent, and expansion patterns. (3) The temporal variation, which highlights inter- and intra-annual changes in the dynamics of mariculture. To investigate the extent of the expansion of the mariculture, the increase in the area per grid time period was determined and analysed. In each grid cell, the proportion and variation of types of mariculture were also examined. The degree of expansion for each grid was determined using the following expression:

$$E = \frac{\Delta y}{S} \times 100 \quad (1)$$

where Δy represents the change in the mariculture area of each grid, and S is the area of the grid. A negative E value indicates a decrease in the mariculture area in a grid, whereas a positive value represents an increase.

We propose to analyse the spatial and temporal distribution of mariculture using centre-of-gravity migration methods in order to further investigate the spatial and temporal dynamic processes of mariculture. The geometric centre of gravity migration trajectory of mariculture data in the study area from 2013 to 2021 was calculated in ArcGIS 10.2 [53], and this is based on the following expression:

$$d_i^t = \sqrt{(X_i - X^t)^2 + (Y_i - Y^t)^2 + (Z_i - Z^t)^2} \quad (2)$$

where X_i, Y_i , and Z_i are coordinates for feature i and n is the number of features.

The ArcGIS 10.2 was then used to estimate transitions between mariculture types based on changes in the classification attributes of each raster cell for 2013–2018 and 2018–2021. The size of each raster cell was 30 m \times 30 m, and the classification codes (1–8) were recorded in the attribute table that was used to interpret the remote sensing data. Each raster cell was attributed a three-digit value based on Equation (3), and these corresponded to the classification codes of a cell for 2013, 2018, and 2021. The property sheet of the raster data also records the number of grids encoded in three digits. By multiplying the number of grids by the area of a single grid, the area variation corresponding to the three-digit code can be obtained. After processing the raster attribute data, visual mapping was performed to highlight the transformations of marine cover types. The raster cell values were obtained using the following equation:

$$N = 100 * C_{2013} + 10 * C_{2018} + C_{2021} \quad (3)$$

where N is the raster result and C_{2013} , C_{2018} , and C_{2021} are corresponding remote sensing interpreted data codes for 2013, 2018, and 2021.

In order to explore the spatial variation in hot spots among different mariculture types, ArcGIS10.2 was used to calculate the change frequency of mariculture types at the pixel scale in the study area from 2013 to 2021. The calculation formula is similar to Equation (3), but the difference is that the classification data of nine remotely sensed images from 2013 to 2021 are calculated. The statistics of change frequency are conducted in Excel 2019.

2.2.3. Analysis of Driving Forces of Mariculture Change

As shown in Table 1, 13 criteria including mariculture, geographical, and anthropogenic factors were utilised, following a consideration of the accessibility of data and the findings of previous studies [17,54–56]. The mariculture and geographical factors were calculated primarily based on the interpretation of remote sensing data. Anthropogenic factors were investigated using night light data, and the data utilised in the present study involve the monthly average from January 2015 to December 2021. The annual night light data were then obtained via a summation of the monthly data, and the mean and total values in a buffer (5 km) were calculated by using data from the centre of each grid.

Table 1. Primary driving factors of changes in mariculture.

Categories	Code	Name	Unit	Detail
Mariculture	F1	area_init	m2	the initial area of the mariculture, which reflects the potential for the further expansion of a grid
	F2	num_type	pcs	the initial number of mariculture types per grid cell
	F3	num_c_type	pcs	the change in the number of mariculture types per grid cell
	F4	dis_land	m	the centre of the geometric grid closest to the land at the beginning
	F5	dis_island	m	the distance from the nearest island
Geographical factors	F6	dis_scell	m	the distance between each grid and its closest neighbours involving the same type of mariculture
	F7	dis_c_scell	m	the change in the distance between each grid and its closest neighbours involving the same type of mariculture
	F8	dis_dcell	m	the distance between each grid cell and its closest neighbours involving a different type of mariculture
	F9	dis_c_dcell	m	the change in distance between each grid cell and its closest neighbours involving a different type of mariculture
	F10	sum_init_light	Nano	the sum of the night light data for an area > 5 km ²
Human Factors	F11	sum_c_light		the change in the sum of the night-time lighting data
	F12	ave_init_light	Watts	the average of the night light data for an area >5 km ²
	F13	ave_c_light	/cm2/sr	the change in the average of night-time lighting data

GeoDetector was utilised to analyse potential factors that control changes in mariculture. Considering that the GeoDetector method deals with just discrete variables, the 13 criteria were transformed into discrete variables [41]. These variables were then subsequently categorised using five classes (1–5). The factor detector and interaction factor detector were chosen in the present study to highlight factors driving changes in mariculture. The factor detector identifies factors that are responsible for an independent variable, and the explanatory power (q) of each factor was obtained from the following expression:

$$q = 1 - \frac{\sum_{h=1}^L N_h \delta_h^2}{N \delta^2} \quad (4)$$

where q is the explanatory power of a factor on changes in the area of mariculture, h is the number of classifications or partitions of Y or factor X , N_h and N are the units in class h and the entire region, respectively, and δ_h^2 and δ^2 are correspondingly variances of Y for units in class h and the entire region. The values of q range from 0 to 1, and the spatial heterogeneity of Y increases as q increases. The noncentral F-test was used to determine the significance of the q values [40].

Conversely, the interaction detector assesses if the explanatory powers of two factors are enhanced, weakened, or independent of each other. The relationships between two factors can be categorised as presented in Table 2.

Table 2. Summary of criteria and categories associated with the interaction detector.

Criteria	Interaction
$q(x1 \cap x2) < \min(q(x1), q(x2))$	weaken–nonlinear
$\min(q(x1), q(x2)) < q(x1 \cap x2) < \max(q(x1), q(x2))$	weaken—univariate
$q(x1 \cap x2) > \max(q(x1), q(x2))$	enhance—bivariate
$q(x1 \cap x2) = q(x1) + q(x2)$	independent
$q(x1 \cap x2) > q(x1) + q(x2)$	enhance—nonlinear

2.3. Data Sources

In the present study, the Sentinel-2 and Landsat 8 OLI data (Table A2) were obtained from GEE, whereas the night light data (NPP-VIIRS) were retrieved from the LAADS DAAC platform (<https://ladsweb.modaps.eosdis.nasa.gov/search/>) [57]. In addition, shoreline data and the documents *Detailed Mariculture Control Plan of Zhao'an County* (2020–2030) and *Dongshan County Mariculture Waters and Mudflats Plan* (2018–2030), were provided by the Zhangzhou Ecological Environment Bureau. Other mariculture-related policy information was obtained from the Department of Ecology and Environment of Fujian Province (<http://sthjt.fujian.gov.cn/>).

3. Results

3.1. Spatiotemporal Dynamics in Mariculture

The classifications associated with the aquaculture information that were extracted from remote sensing data were: producer's accuracy values were >85%, user's accuracy values were >89%, overall accuracy values were >85%, and the kappa coefficients were >0.9 for all years, excluding 2015 (0.83) (Tables A3 and A4). Through field and human–computer interaction verification, the classification accuracy value was >80% (Table A5). The dynamics of mariculture in Zhao'an Bay from 2013 to 2021 are depicted in Figure A1 and Figure 4. The spatial resolution of annual scale classification results obtained based on Landsat 8 OLI is 30 m (Figures 4 and A1). The spatial resolution of the seasonal scale classification results obtained based on Sentinel-2 is 10 m. In general, raft mariculture, which covers the largest area, is prevalent throughout the bay. This is the main mariculture at the inlet of the bay, whereas cage mariculture, which is also common in the bay, is prominent around the islands. Notably, from 2013 to 2020, cage mariculture was distributed in the northeast of Zhao'an Bay, and it disappeared after 2020. The main cage and pond mariculture are in Dongshan County, whereas the principal raft and mudflat are in Zhao'an County.

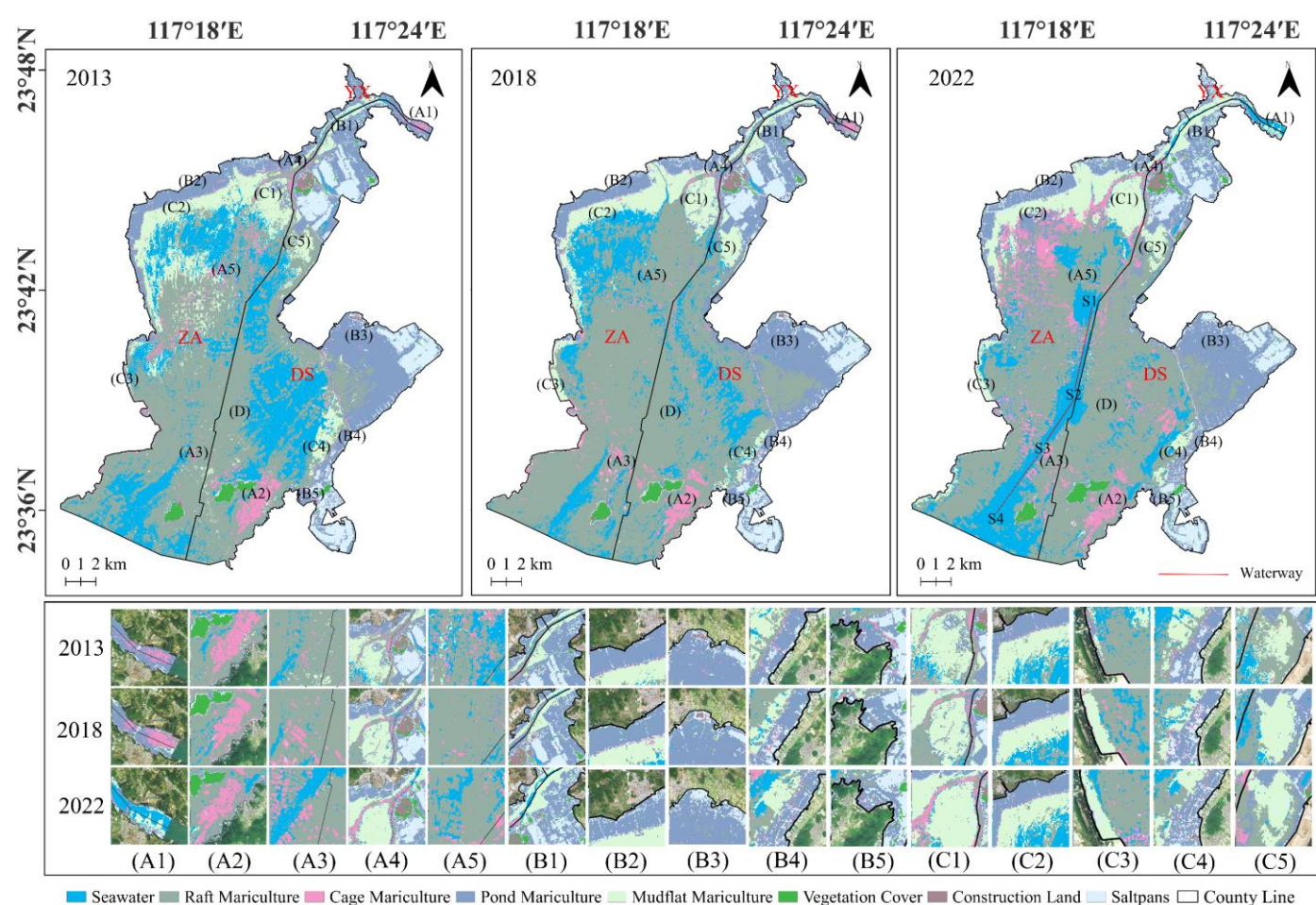


Figure 4. Maps showing results from the interpretation of remote sensing data for the study area for 2013, 2018, and 2022. The cage is represented by letters A1 to A5, whereas the pond is denoted by letters B1 to B5, the mudflat by letters C1 to C5 and the raft by letters D. The waterway is shown by the line from S1 to S4 on the 2022 map that was derived from remote sensing data.

Additionally, Figure A2 displays the spatiotemporal dynamics of different maricultures through the geometric centre of gravity. In the period from 2013 to 2021, the geometric centre of gravity for raft mariculture shifted to the northeast of the bay, whereas that for cage mariculture significantly shifted from 2013 to 2016 and slightly from 2017 to 2021.

Considering the availability of remote sensing images, classification accuracy, and mariculture management policies, the transition from one mariculture to another was investigated in the period from 2013 to 2018 and 2021 in the bay, and the results are depicted in Figure 5. Notably, raft mariculture occupies the largest area and the main interconversion with the seawater, but some interconversion with the pond, mudflat, and cage also occurred during the period from 2013 to 2021. Compared to the period from 2018 to 2021, the amount of saltwater converted to raft mariculture was greater during the period from 2013 to 2018. Among the four types of mariculture, the cage occupies the smallest area, and the main conversion is to another cage. Additionally, salt pans were predominantly converted to pond mariculture.

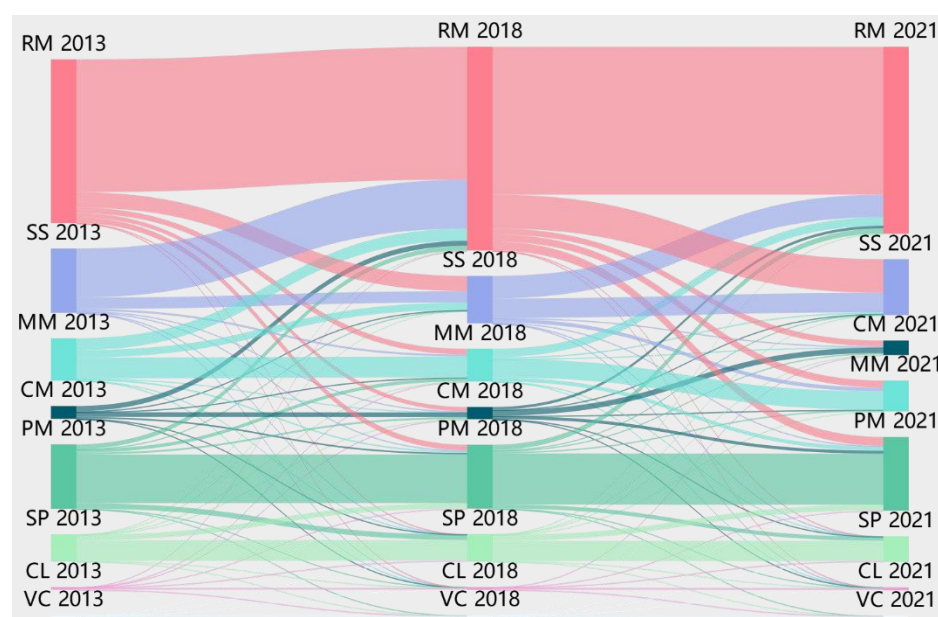


Figure 5. Illustration of transitions among mariculture types in Zhao'an Bay from 2013 to 2021. RM: raft mariculture, SS: seawater surface, MM: mudflat mariculture, CM: cage mariculture, PM: pond mariculture; SP: salt pan, CL: construction land, VC: vegetation cover.

The expansion of the major types of mariculture during the periods 2013–2018, 2018–2021, and 2013–2021 was also examined at the grid scale, and the results are shown in Figure A3–6. According to Figure A3, raft mariculture increased from 2013 to 2018, but decreased from 2018 to 2021, with an overall positive expansion during the 2013–2021 period. Figure A4 reveals a pattern similar to that of the raft for cage mariculture, but the expansion of the latter is higher relative to the former. Figure A5 shows that even though pond mariculture declined from 2013 to 2018, the increase from 2018 to 2021 produced an overall expansion for the 2013–2021 period. In contrast, Figure A6 demonstrates that because of the decrease in mudflat mariculture from 2013 to 2018, despite the increase from 2018 to 2021, this mariculture type contracted for the 2013–2021 period. Notably, the proportion of unchanged mudflat mariculture exceeds 50%.

The change frequency of different mariculture types during the periods 2013–2021 was also explored at the pixel scale, and the results are shown in Figure A7. According to Figure A7, the places with high change frequency include the seaway, bay mouth, the sea near the land, etc., whereas the ponds, islands, salt farms, and the middle of the bay suffered from little change.

The spatial and temporal variations in county-level mariculture from 2013 to 2021 are shown in Figures 6 and A8. Evidently, raft and mudflat mariculture are prevalent in Zhao'an County, whereas cage and pond mariculture are dominant in Dongshan County. Concerning changes occurring during the period from 2018 to 2021 in both Dongshan and Zhao'an Counties show an 'increasing–decreasing–increasing' pattern, even though the rates of these changes in the latter are higher than in the former.

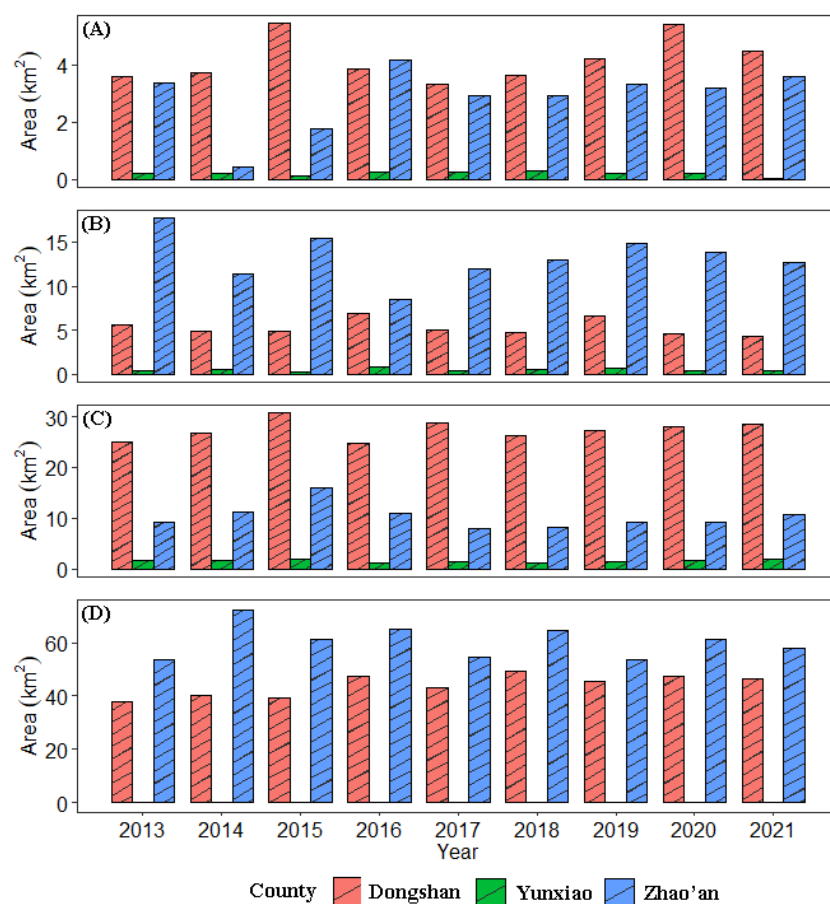


Figure 6. Plot showing changes in types of mariculture in different counties during the period from 2013 to 2021 including the (A) CM, (B) MM, (C) PM, and (D) RM.

In Figure 7, inter-annual variations of different types of mariculture are displayed. The mariculture area, including the pond, raft, mudflat, and cage, increased by 7.5% from 2013 to 2021, even though mudflat mariculture decreased by 33.66%. Raft mariculture occupies the largest area during this period, followed by cage mariculture, whereas pond and mudflat mariculture exhibit insignificant changes.

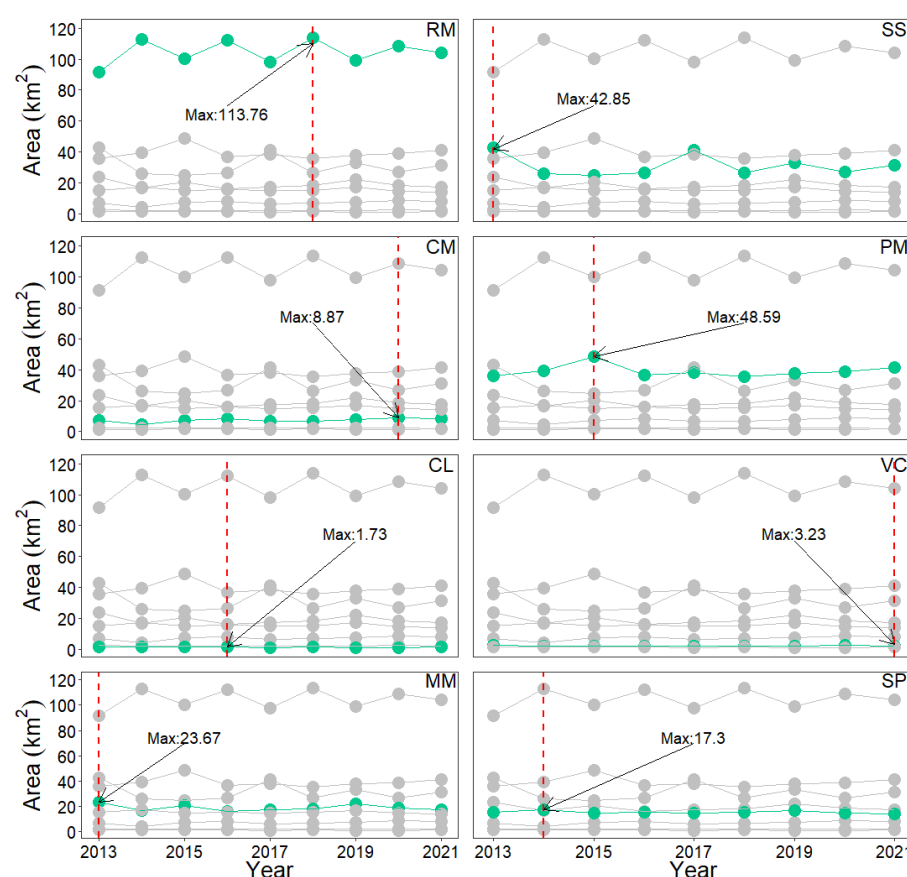


Figure 7. Plot showing inter-annual variations of aquaculture types in Zhao'an Bay from 2013 to 2021.

Seasonal variations in the dynamics of mariculture in Zhao'an Bay were also investigated, and the results are shown in Figure 8. Cage mariculture increased by 60.11% from the winter of 2015 to the spring of 2022, and the period between the winter of 2015 and the spring of 2019 was characterised by a rapid increase. Overall, mudflat mariculture was essentially unchanged, except for a notable increase of 30.5% from the spring to the autumn of 2020. Sea water is characterised by an overall decrease. Further, raft mariculture increased throughout the period studied, but the period from the spring of 2017 to the autumn of 2020 is characterised by minor changes followed by a significant increase in area. Changes in the ponds reached a maximum in the spring of 2016, and overall, they exhibited minimal variations.

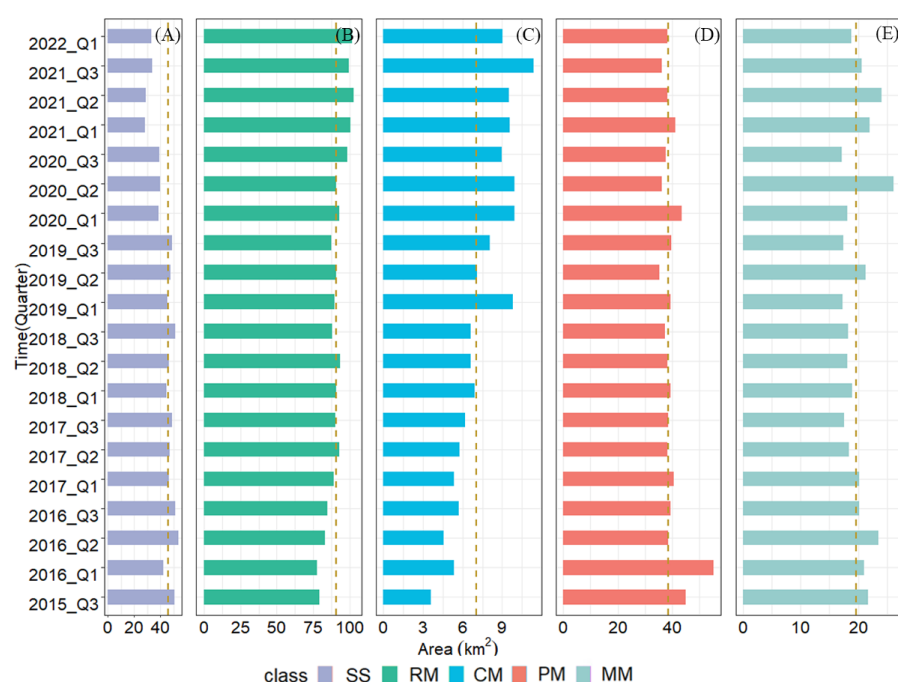


Figure 8. Plot showing seasonal variations of types of mariculture in the Zhao'an bay including Q1: spring (March–May), Q2: autumn (Sep–Nov), Q3: winter (Dec–Feb). (A) Sea water; (B) Raft mariculture; (C) Cage mariculture; (D) Pond mariculture; (E): Mudflat mariculture. Note: seasonal scale data for mariculture in summer (June–August) are excluded because of the high cloudiness associated with the remote sensing data and the fishing moratorium during this period.

3.2. Potential Driving Factors of Mariculture Expansion

Drivers of changes in mariculture in Zhao'an Bay from 2013 to 2021 are displayed in Figure 9. Notably, grids with a small initial area (F1) exhibit the potential to expand for all types of mariculture, excluding the raft. Additionally, geographical factors (F4–F9) clearly impact all four types of mariculture. Even though all types of mariculture are also influenced by human factors (F10–F13), ponds display the highest impact. Human factors exert more influence on these changes as the variation in night-time lighting increases (F11, F13). Variables driving changes in various mariculture areas were estimated using GeoDetector, and these data are presented in Table A6 (see Table 1 for details on driving factors).

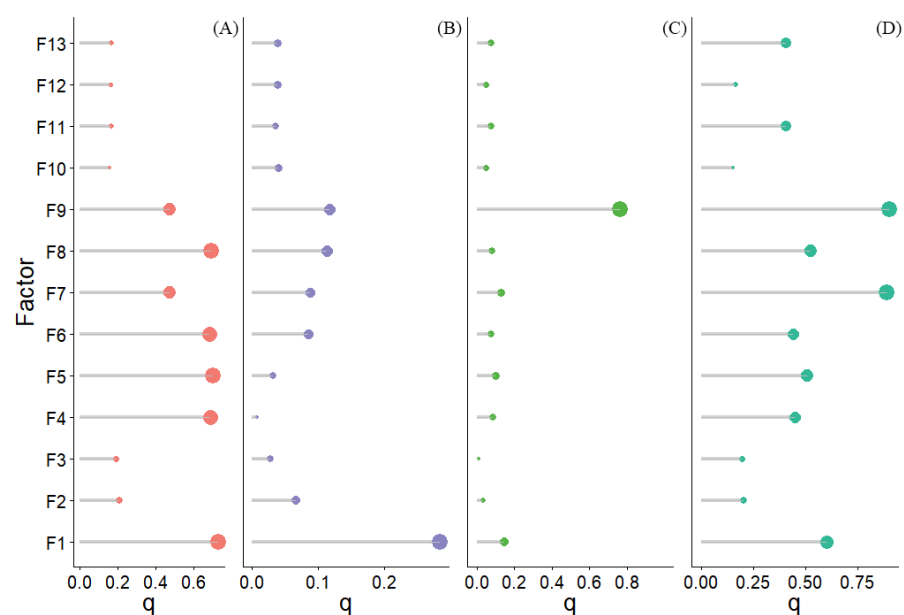


Figure 9. Plot displaying drivers of changes in types of mariculture including the (A) raft, (B) cage, (C) pond, and (D) mudflat.

Figure 10 demonstrates that the interaction q value of a factor pair is superior to that of the individual factors. The 62 factor pairs in cage mariculture exhibit strong correlation and enhancements. All combination pairs for the mudflat, pond, and raft also display enhancement. Notably, the F1 and F9 combination for pond mariculture is characterised by a nonlinear enhancement.

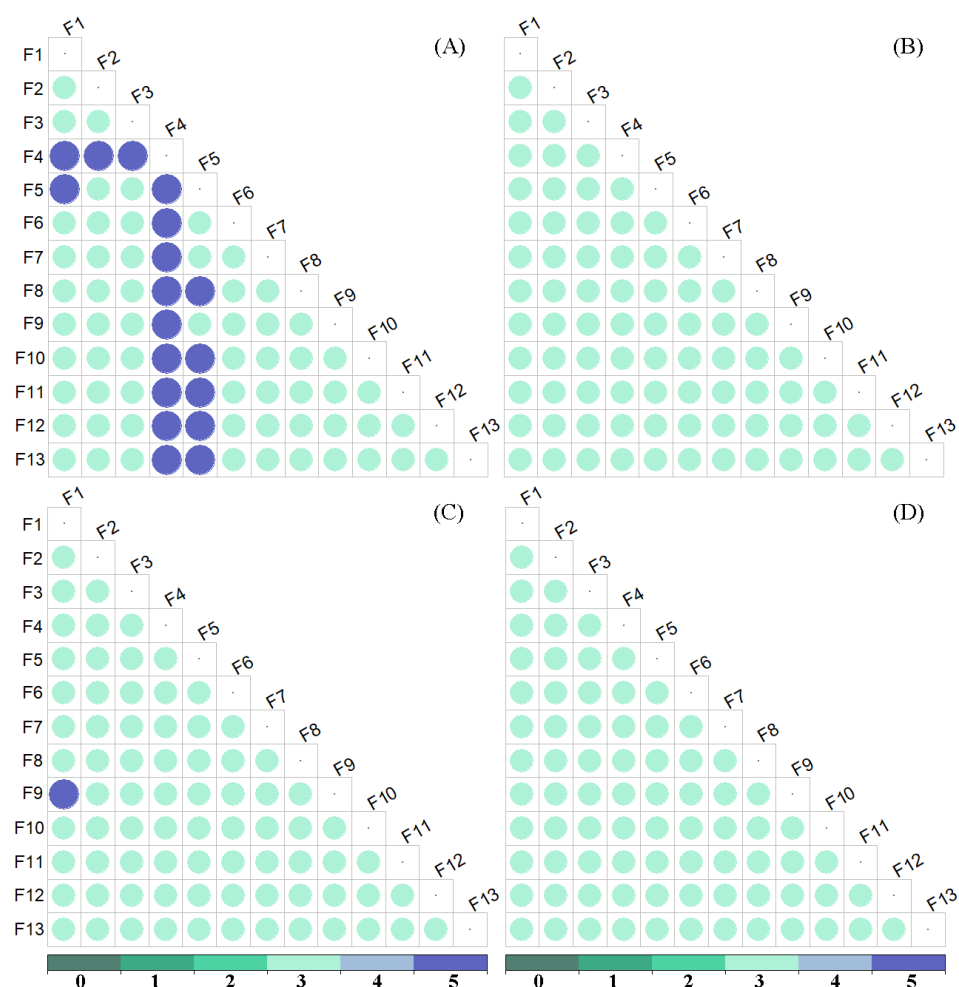


Figure 10. Plot showing results of the interaction detection for (A) cage, (B) mudflat, (C) pond, and (D) raft. 0: self-intersection; 1: weaken, nonlinear; 2: weaken, univariate; 3: enhance, bivariate; 4: independent; 5: enhance, nonlinear.

4. Discussion

4.1. Effectiveness of the Proposed Method

The present study illustrates the effectiveness of integrating the GEE online cloud platform and GeoDetector to monitor mariculture and its drivers in Zhao'an Bay. The proposed method produces acceptable classification accuracy, with an overall accuracy over 85% and a kappa coefficient of 0.8 (see Appendix B for details regarding the accuracy of the remote sensing image classification results). According to the USGS and existing studies, an overall accuracy and kappa coefficient of 80% are adequate [58]. Compared to the traditional methods, the proposed approach has its advantage in pre-processing raw remotely-sensed images and extracting mariculture features due to its powerful function of cloud computing [23,24]. Existing GEE-based mariculture extraction studies are mainly on individual types [15,16]. In the present study, four types of mariculture were extracted simultaneously using the GEE platform. In this proposed method, we also developed a computational index to identify the submerged raft mariculture from images using the conventional combination of bands (Figure 3). Furthermore, we demonstrate that the mariculture, geographic factors, and anthropogenic factors all significantly contribute to the expansion of mariculture using GeoDetector. The main drivers differ among the type of mariculture and might be associated with the implementation of mariculture management policies. For example, mariculture was prohibited in the waterway and other areas of concern (e.g., gauge of seawater quality) in Zhao'an Bay. This intervention was intended to limit damage to ecosystems in the bay that can be caused by increasing human

demands. The present study has implications for local mariculture planning in the bay and for the development of policies to protect its ecosystems.

4.2. Pattern of Mariculture Dynamics

Spatiotemporal dynamics of mariculture in Zhao'an bay were exhibited at different scales. Different types of mariculture were associated with unique spatial distributions and specific annual- and seasonal-scale characteristics during the study period, and these observations are consistent with other studies [17,45,59–61]. The present study revealed that the area associated with seafood mariculture in Zhao'an Bay increased by 7.5% (12.74 km²) during the period from 2013 to 2021. This increase is attributed primarily to the increase in global demand for seafood, which is similar to other observations [15,17]. Raft mariculture is present throughout the bay, whereas cage mariculture is common near islands (Figures 4 and A1). These two types of mariculture occupy approximately two-thirds of the mariculture area in Zhao'an Bay, and these control the layout of the mariculture industry in Zhao'an Bay, which was confirmed through field surveys. These results highlight the trial-and-error approach of integrated multi-trophic aquaculture (IMTA) [62] in the practice of mariculture in Zhao'an Bay. Owing to synergistic interactions between species, the IMTA refers to the mariculture of species at different nutrient levels, which allows the capture and conversion of the unconsumed feed, waste, and by-products of one species into fertiliser, feed, and energy for other species [62]. This model optimises the socio-economic benefits of mariculture, reduces feed costs, and mitigates its negative environmental impacts.

In Zhao'an Bay, ponds and salt pans are frequently adjacent, and thus, the interconversion of this mariculture is common (Figures 4 and A1). However, this differs from the rapid expansion of ponds in other areas, which is attributed to the conversion of mudflats and cultivated land [63]. The dominance of raft and mudflat mariculture in Zhao'an, as opposed to the cage and pond mariculture prevalent in Dongshan County (Figures 6 and A8), is associated with the local demand for seafood and farming habits. The rate of change in raft mariculture in Zhao'an County is higher than in Dongshan County, mainly because of the frequent conversion between mudflats and rafts in the former and the prohibition of mariculture in the waterway in 2022. Figure A7 shows that the types of mariculture in the seaway, bay mouth, and sea near land have a high frequency of changes at the pixel scale, which is mainly due to the great influence of human activities.

Figure A2 shows that the migration path for the centre of gravity of pond and mudflat mariculture minimally changed, which indicates no major change in areas occupied by these types of mariculture in the bay during the study period. According to previous studies, the large-scale reclamation of coastal areas used for mariculture in China started in 2000, and this subsequently attained stability [64]. Consequently, the geometric centre of gravity for cage mariculture shifted from the inlet to the interior of the bay, and this can alter the pollution centre in the bay.

Owing to the increasing demand for food by humans, both raft and cage mariculture increased from 2013 to 2021. This is associated with the increased demand for seafood and its economic benefits [30]. However, approximately 50% of grids associated with cage mariculture are unchanged, and this indicates some stability in their positions. In addition, pond mariculture is characterised by a segment of continuous decline (2013–2018), but this increased overall from 2013 to 2021. This overall increase in pond mariculture is consistent with the results of existing studies [63], and the decrease observed is likely because of the conversion of ponds to salt pans. Previous studies on changes in mariculture are commonly based on an annual scale [58,65,66,66], and thus, in the present, seasonal patterns were investigated. The present study shows that the area occupied by cage mariculture in the winter is greater than that in the spring and autumn (Figure 8). Mudflat mariculture exhibits a seasonal consistency, which involves a smaller area in the winter than in the spring and autumn. Conversely, the area linked to raft mariculture is lower in the autumn and winter. Interestingly, from winter in 2015 to spring in 2022, no seasonal

change in the area occupied by pond mariculture was noticed. We found that cage culture and mudflat mariculture showed large fluctuations in spring 2019 and autumn 2020, respectively. The main reason is the balance between environmental protection and economic development. The Ministry of Ecology and Environment of the People's Republic of China informed Zhao'an Bay in 2019 that the water quality was rated as class IV, which denotes poor water quality [67]. To solve this problem, the local government has regulated mariculture in Zhao'an Bay [68], but in the pursuit of economic benefits, the cage area increased again in the winter of 2019. Similarly, in 2020, Zhao'an Bay cleaned up cage mariculture again, but the area of mudflats increased accordingly [69].

4.3. Main drivers of Mariculture Dynamics

The large-scale development of mariculture is closely related to economic growth, demand for seafood, and the expansion of infrastructure [39,70]. Changes in the area associated with mariculture are driven by a combination of types of mariculture, geographic factors, and anthropogenic factors (Figures 9 and 10). The main driving factors differ according to the types of mariculture, and this observation is consistent with results from previous studies [17,38].

The present study suggests that a larger initial mariculture area requires more financial resources and a greater capacity to build farming infrastructure. This highlights a strong capacity for expansion, which is consistent with findings from previous studies [38]. In addition, the farther mariculture units are from land and islands, the less likely the influence of humans. Therefore, space for expansion is higher, which increases the chances of transforming these units into a major mariculture area. Human activities significantly impacted mudflat mariculture, and the occupied area increased as the mean and total night-time light increased. The combination of two driving factors also affected changes in the mariculture area more than one factor alone (Figure 10). The interaction between the influencing factors enhances their effects on changes in mariculture, and this is also consistent with results from previous studies [13,17,43,71].

Furthermore, local government policies enhanced the development of mariculture. In 1985, for example, Fujian Province introduced the *Outline of the Construction of Eight Bases*, which focused on the development of shallow mudflat mariculture. In 1996, Fujian Province declared aquaculture as a primary industry, and subsequently, large areas occupied by mudflats were utilised for mariculture in other provinces along the coast of China [72,73]. The management of shallow sea mudflat aquaculture in Fujian Province was regulated in 2000, and this facilitated the development and aquaculture-related preparation of abandoned mudflats. In 2002, a law on the use of sea area was introduced [64], and this strengthened regulations on mariculture along the coast of China. Subsequently, the Government of China established policies to promote artificial culture and mariculture technologies. These were intended to accelerate the development of mariculture in the 21st century and to meet the growing demand for mariculture products in society [63].

According to the present study, mariculture occupies >90% of the Zhao'an Bay area, and this is among the major sources of income for residents. However, in 2021, the government introduced ecological protection policies to reduce the damage and impact of mariculture on the water quality and ecosystem in the bay. As shown in Figures A1 and 4, for example, mariculture was eliminated in the west channel of Zhao'an Bay and the north of Bachi Gate. The establishment of new units far from existing mariculture units has been demonstrated to effectively mitigate the negative impacts of a high mariculture density [74]. However, following the introduction of integrated mariculture management by the government in the bay in 2021, the mariculture density increased in some areas because of livelihood pressures (Figures 4 and A1), and these maintained a high pressure on the ecosystem in the bay.

Economic conditions also have significant impacts on the expansion of coastal aquaculture because the increased demand for seafood is highly profitable. In addition to quality, demand for seafood has shifted from seasonal to perennial [75], and this is a potential

factor driving the continued growth of the aquaculture area. Alternatively, aquaculture is characterised by a higher economic efficiency compared to traditional industry and agriculture [76]. Therefore, people are more willing to incorporate aquaculture, especially in coastal areas where water resources are abundant.

4.4. Management Implications and Limitations

To reduce the impact on the utilisation of marine resources while maintaining the livelihood of the population growth and economic development, some recommendations were put forward in China and other nations [77,78]. First, a methodology (model) is developed to explore the interaction of people with the ocean [79,80]. In this approach (model), mariculture systems are considered a product of the coupling of human and marine systems, and thus, human development is integrated into the conservation of marine systems. Second, an integrated monitoring and assessment of the socioeconomic benefits and environmental impacts of mariculture on the bay is necessary. Through this approach, the effects of different types of mariculture on food production and quality, livelihoods, marine ecosystems, etc. can be compared [81,82]. In such an endeavour, the internet, the Internet of Things, cloud computing, artificial intelligence, machine learning, and big data analytics must all be exploited [83–87]. Third, spatial planning policies and programs should be developed for the bay to achieve sustainable development goals, coordinate competing marine areas, and reduce water pollution and pressure on the ecosystem [88–90]. In many studies on spatial planning, the feasibility of monoculture has been crudely assessed [63,91,92]. Therefore, studies on interactions between multiple types of mariculture and mariculture areas can be complementary. In addition, a combination of different types of mariculture in an area can improve planning for the spatial layout of the bay and reduce the associated environmental impacts. Finally, environmental education, scientific mariculture training, improved mariculture infrastructure, the production of high-quality feed, and feed use management can all improve mariculture practices. Long-term sustainable use of marine ecosystems can be achieved through an improved understanding and management of human–ocean interactions.

The present study, however, involves few limitations. First, the Landsat 8 OLI and Sentinel-2 imagery data obtained from the GEE platform lacked data for June, July, and August during the study period, which to some extent influenced the identification of the spatiotemporal distribution of mariculture dynamics in this study. Second, influencing factors such as the COVID-19 epidemic may be further involved.

5. Conclusions

Investigating the pattern of mariculture and its drivers is crucial for local mariculture planning and eco-environment protection. Previous efforts in the dynamic monitoring of bay mariculture required downloading remotely sensed images to a local computer for processing, which consumes more time and requires a higher requirement of hardware. To address these issues, the GEE online cloud platform was utilised to capture changes associated with different types of mariculture in Zhao'an Bay in the present study. The associated drivers and the extent to which these contribute to changes in mariculture were determined using GeoDetector. The combination of GEE and GeoDetector facilitates the rapid realisation of dynamic monitoring and driving force analysis of bay mariculture. Distinct spatiotemporal variations in mariculture dynamics were exhibited in Zhao'an bay over time. Mariculture products for human consumption were identified as the major drivers. To achieve the sustainability of the bays, we need to balance development and conservation with sound approaches to clearly understand the pattern and drivers of mariculture dynamics locally. This may be a popular solution for similar coastal bays with intensified anthropogenic disturbance.

Author Contributions: Conceptualisation, P.W. and J.H.; Data curation, P.W., J.W., and X.L.; Methodology, P.W., J.W., X.L., and J.H.; Resources, P.W., J.W., and X.L.; Writing—original draft, P.W.;

Writing—review and editing, P.W. and J.H. All authors have read and agreed to the published version of the manuscript.

Funding: This research was funded by the Fujian Environmental Protection Science and Technology Plan Project under Grant 2022R007, and the APC was funded by this project.

Institutional Review Board Statement: Not applicable.

Informed Consent Statement: Not applicable.

Data Availability Statement: Not applicable.

Acknowledgments: We would like to thank the Zhangzhou Municipal Ecology and Environment Bureau for providing data that were relevant to this study. We are also grateful to Google for providing access to the Google Earth Engine platform, which enabled the processing of remote sensing data.

Conflicts of Interest: The authors declare no conflicts of interest.

Appendix A

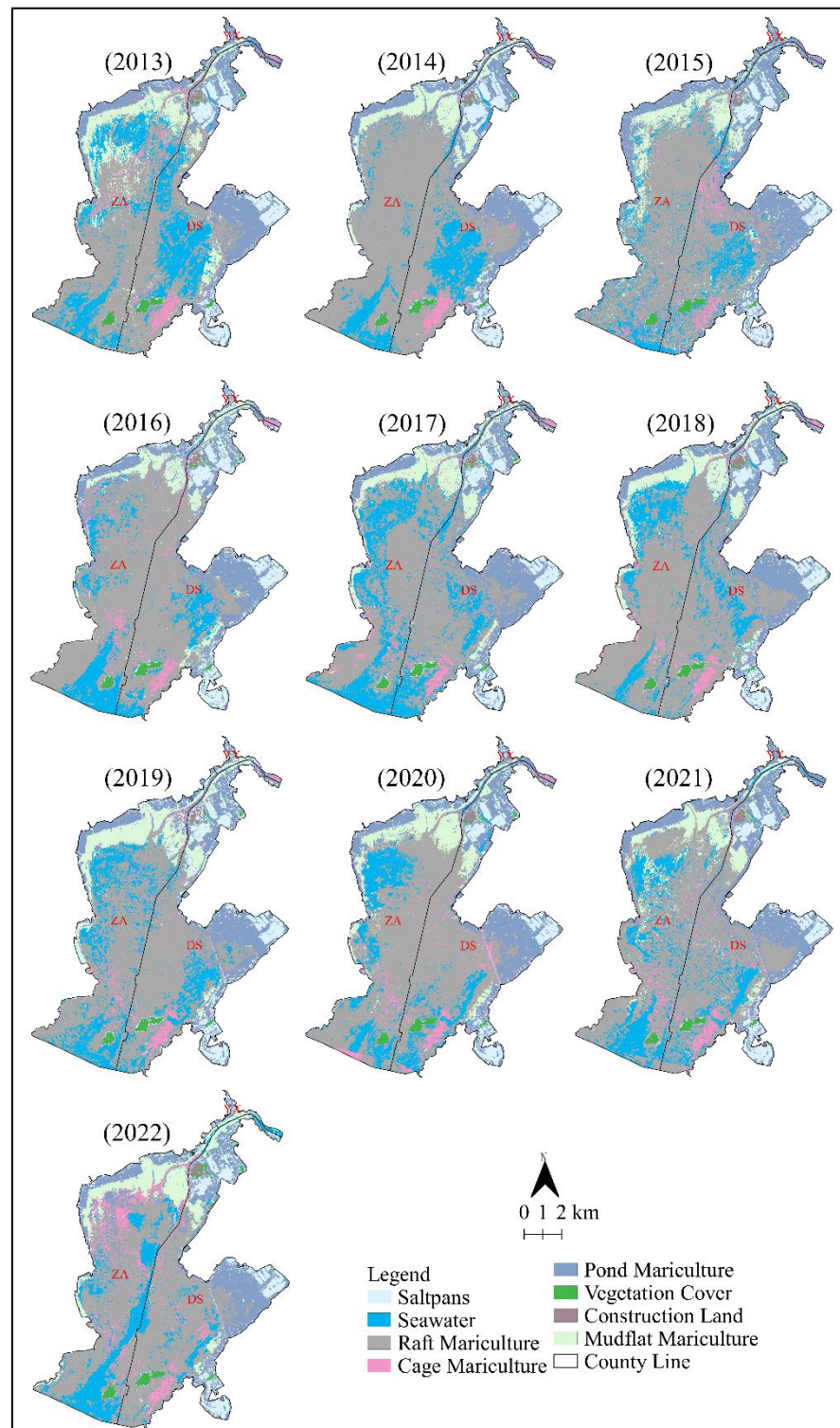


Figure A1. Map highlighting the distribution of mariculture types in the study area from 2013 to 2022 based on remote sensing data.

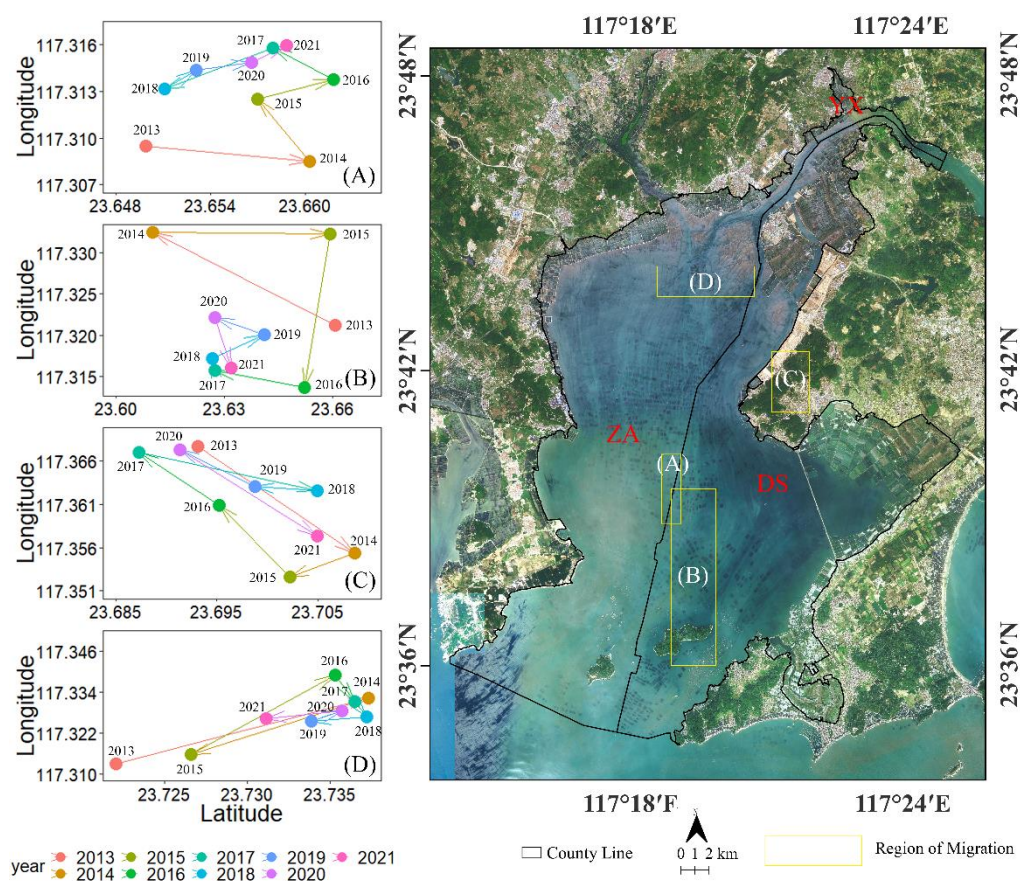


Figure A2. Plot showing migration of the centre of gravity from 2013 to 2018 for different types of mariculture in the study including (A) cage, (B) raft, (C) pond, and (D) mudflat mariculture.

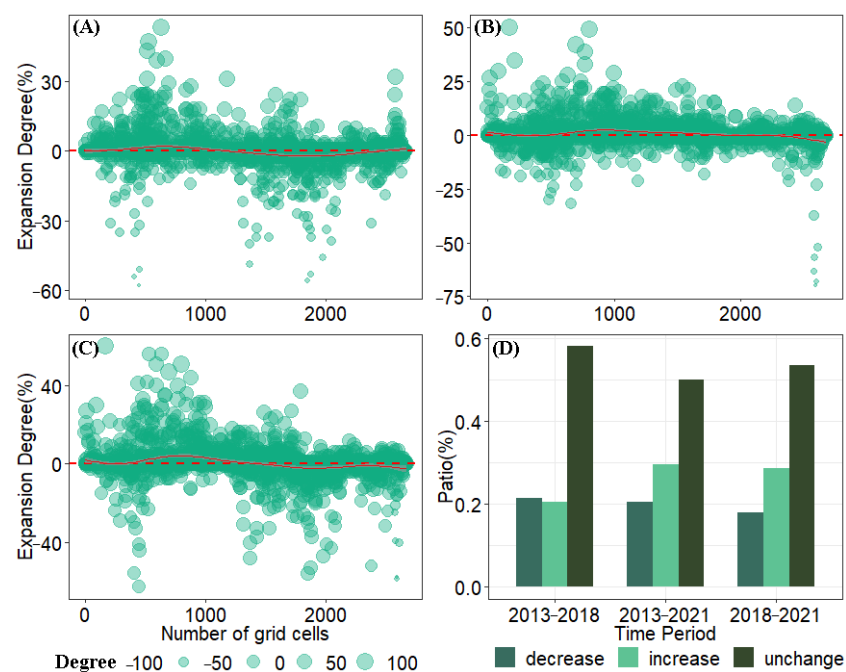


Figure A3. Plot showing the expansion of raft mariculture in the study area at the grid scale including (A): 2013–2018, (B): 2018–2021, (C): 2013–2021, and (D): Ratio changes in raft mariculture during the different periods.

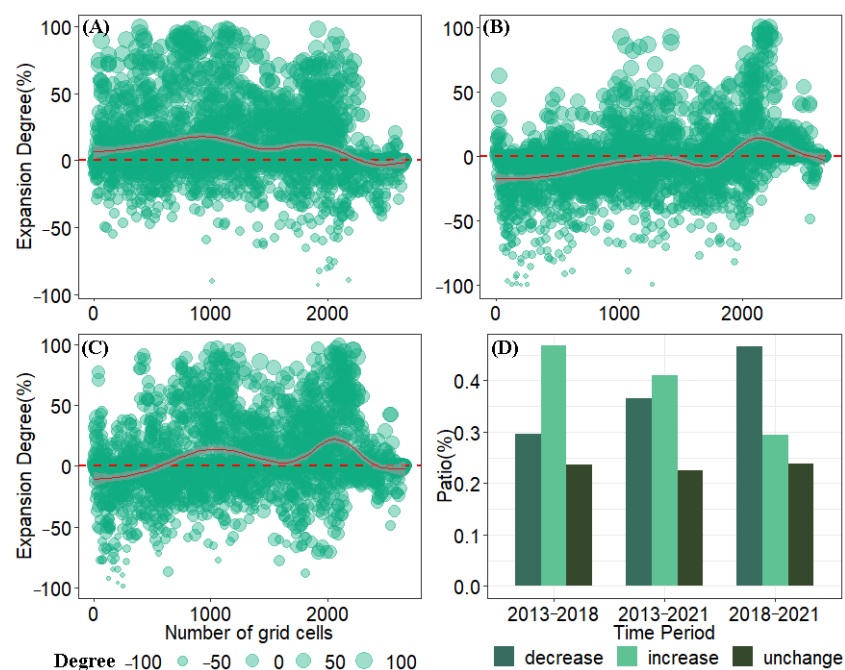


Figure A4. Plot showing the expansion of cage mariculture in the study area at the grid scale including (A): 2013–2018, (B): 2018–2021, (C): 2013–2021, and (D): Ratio changes in cage mariculture during the different periods.

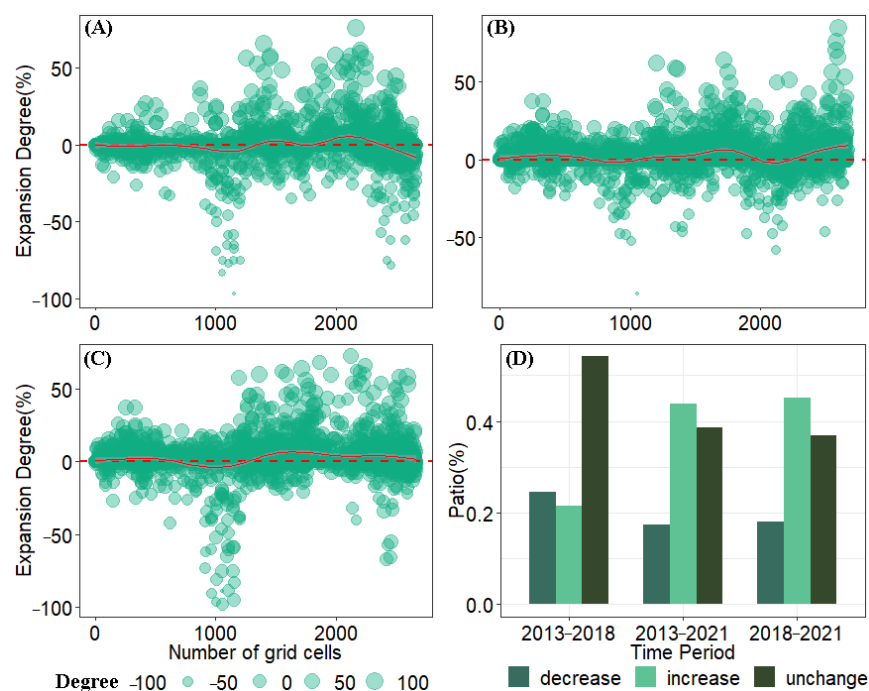


Figure A5. Plot showing the expansion of pond mariculture in the study area at the grid scale including (A): 2013–2018, (B): 2018–2021, (C): 2013–2021, and (D): Ratio changes in pond mariculture during the different periods.

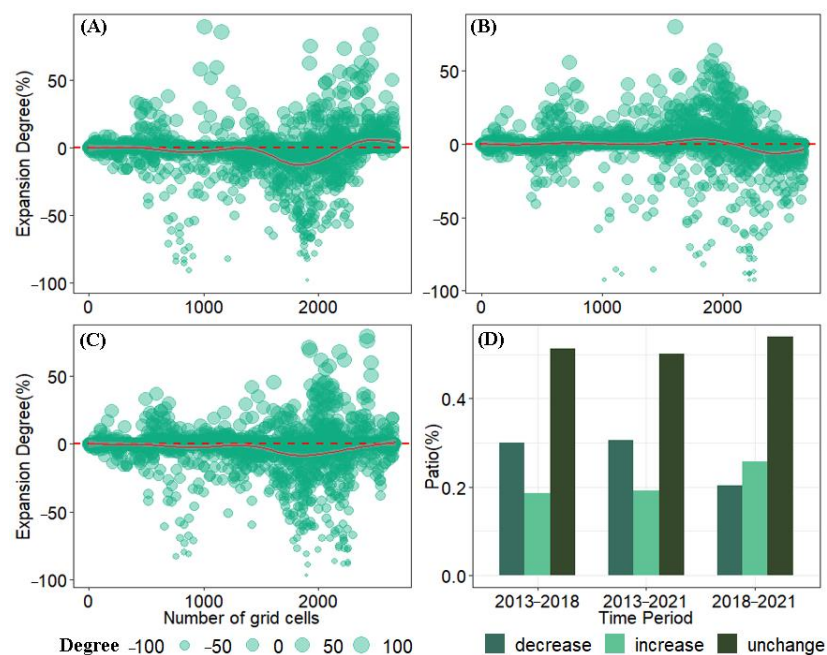


Figure A6. Plot showing the expansion of mudflat mariculture in the study area at the grid scale including (A): 2013–2018, (B): 2018–2021, (C): 2013–2021, and (D): Ratio changes in mudflat mariculture during the different periods.

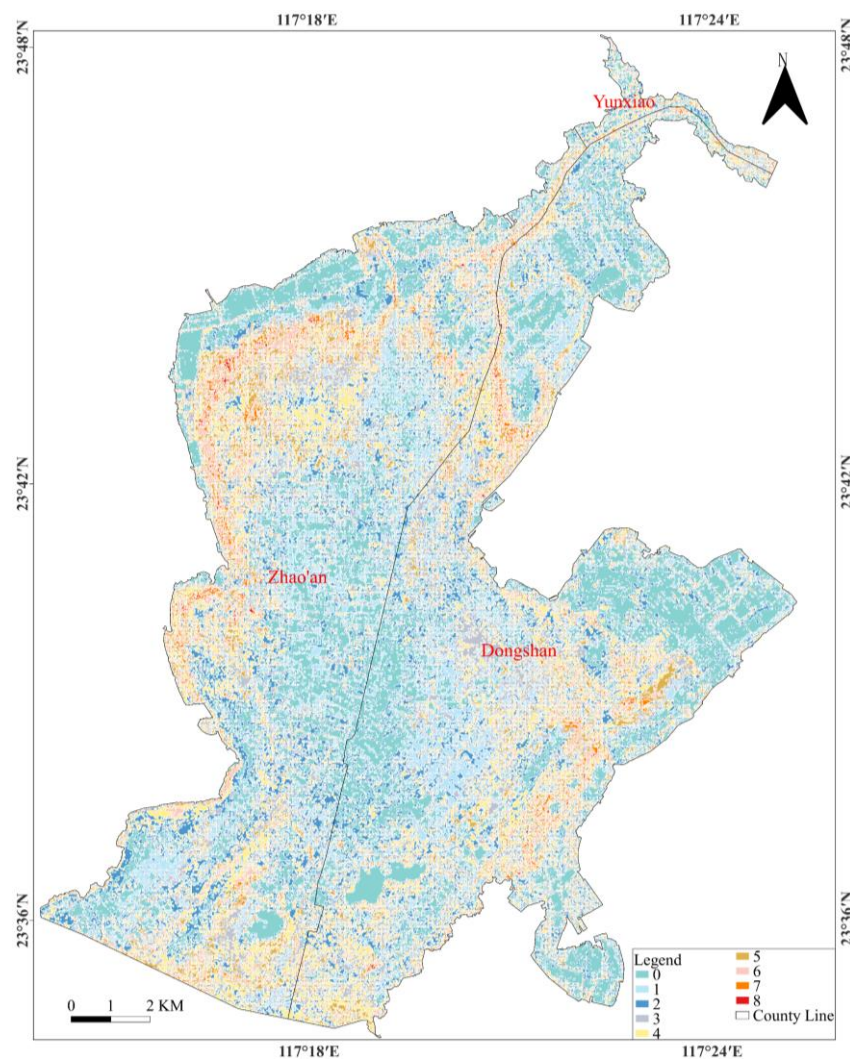
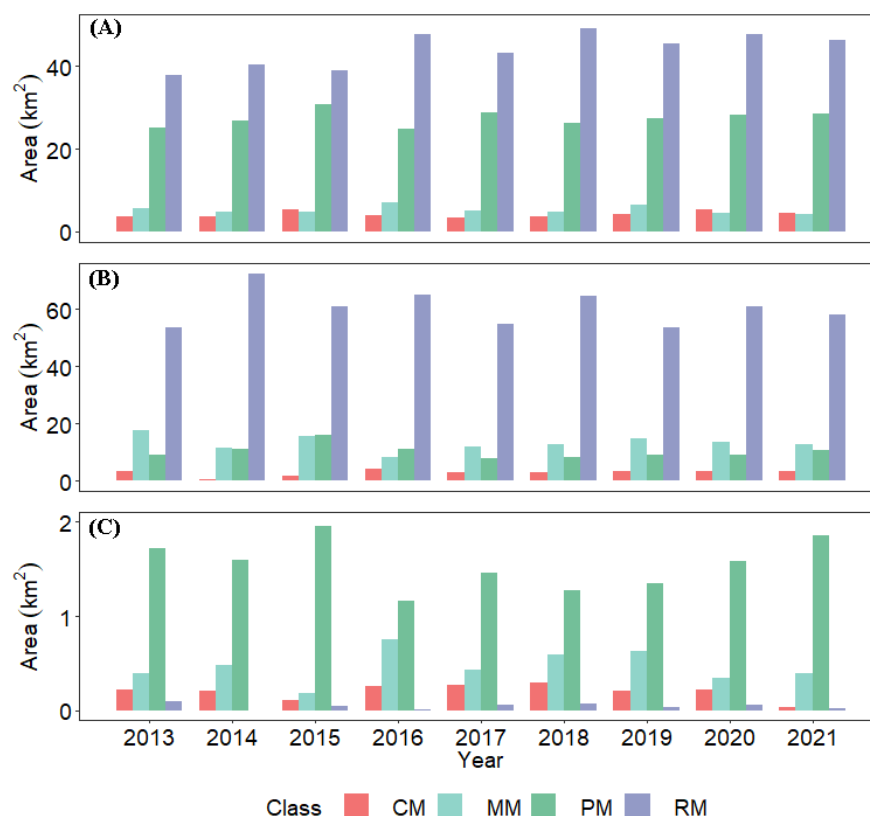


Figure A7. Pixel-scale change frequency of different mariculture types from 2013 to 2021.**Figure A8.** Plot showing changes in maricultural in counties in the study area including (A): Dongshan, (B): Zhao'an, and (C): Yunxiao.

Appendix B

Table A1. Remote sensing interpretation marks.

Land Cover Type	Distribution Area	Image Interpretation Key and Remote Sensing Image Feature			
		Landsat 8 OLI		Sentinel-2	
Pond	Distributed in the gulf coastal zone		Regular shape, blue or blue-black colour		Regular shape, green or dark green
Mudflat	Distributed in tidal flats along the coast extending into the sea		With linear borders and is blue-white in colour		With linear borders, the colour is earthen yellow
Raft	It's found all over the bay		Regular shape, dark blue colour		Regular shape, black colour
Cage	It's found all over the bay		Rectangular shape, reddish in colour.		Rectangular shape, dark red in colour
Seawater	It's found all over the bay		The colour is blue		The Colour is green


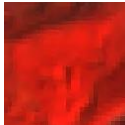
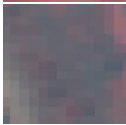
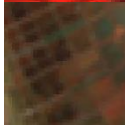

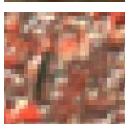
Vegetation cover	Distributed in islands and estuaries		The colour is red		The colour is bright red
Salt pan	Mainly adjacent to the pond		Rectangular shape and dark red in colour		Rectangular shape and dark red in colour
Construction land	Distributed in terrestrial parts of estuaries		No obvious texture, colour mixed grey and reddish		No obvious texture, colour mixed grey and red

Table A2. The band parameter of Landsat 8 OLI and Sentinel-2 satellite remote sensing images used in this study.

Senor	Band Number and Name	Central Wavelength (μm)	Resolution (m)
Landsat 8 OLI	Band1 Coastal	0.443	30
	Band2 Blue	0.483	30
	Band3 Green	0.563	30
	Band4 Red	0.655	30
	Band5 NIR	0.865	30
	Band7 SWIR 2	2.200	30
Sentinel-2 MSI	Band2 Blue	0.490	10
	Band3 Green	0.560	10
	Band4 Red	0.665	10
	Band8 NIR	0.842	10

Table A3. Summary of accuracy values associated with the remote sensing interpretation of the marine cover in the study area.

Year	Overall Accuracy	Producer's Accuracy	User's Accuracy	Kappa Accuracy
2013	0.924	0.904	0.932	0.901
2014	0.951	0.934	0.967	0.934
2015	0.871	0.850	0.901	0.832
2016	0.926	0.914	0.930	0.902
2017	0.923	0.912	0.910	0.9
2018	0.945	0.926	0.941	0.928
2019	0.926	0.858	0.939	0.903
2020	0.940	0.923	0.918	0.922

2021	0.929	0.927	0.899	0.907
------	-------	-------	-------	-------

Table A4. User's accuracy and producer's accuracy of different land cover type in 2013, 2018, and 2021.

Land Cover Type	2013		2018		2021	
	Producer's Accuracy	User's Accuracy	Producer's Accuracy	User's Accuracy	Producer's Accuracy	User's Accuracy
Sea Water	0.817	0.915	0.696	0.946	0.845	0.863
Raft	0.906	0.886	0.974	0.886	0.949	0.886
Cage	0.793	0.913	0.793	0.982	0.793	0.895
Pond	0.967	0.958	0.974	0.959	0.945	0.939
Mudflat	0.923	0.860	0.986	0.956	0.918	0.981
Vegetation Cover	1	0.977	1	1	1	1
Construction Land	0.875	1	1	0.833	1	0.667
Salt Pans	0.951	0.947	0.983	0.963	0.963	0.959

Table A5. Accuracy of field verification of remote sensing image classification results.

Land Cover Type	The Number of Ground Truth Points		Accuracy	
			Landsat 8 OLI	Sentinel-2
Pond	150		0.853	0.866
Mudflat	80		0.801	0.838
Raft	260		0.835	0.840
Cage	100		0.813	0.833
Seawater	80		0.805	0.812
Vegetation cover	20		0.871	0.885
Salt pan	60		0.822	0.850
Construction land	50		0.862	0.878

Table A6. Data for factors (q and p) controlling change in areas for different types of mariculture.

Factors\Name	RM		CM		PM		MM	
	q	p	q	p	q	p	q	p
F1	0.731	0.000	0.28	0.000	0.146	0.000	0.601	0.000
F2	0.207	0.000	0.284	0.000	0.035	0.000	0.205	0.000
F3	0.188	0.000	0.066	0.000	0.013	0.000	0.195	0.000
F4	0.690	0.000	0.027	0.000	0.087	0.000	0.447	0.000
F5	0.705	0.000	0.007	0.048	0.098	0.000	0.509	0.000
F6	0.687	0.000	0.032	0.000	0.076	0.000	0.442	0.000
F7	0.476	0.000	0.085	0.000	0.127	0.000	0.890	0.000
F8	0.693	0.000	0.087	0.000	0.081	0.000	0.526	0.000
F9	0.476	0.000	0.113	0.000	0.764	0.000	0.901	0.000
F10	0.155	0.000	0.116	0.000	0.047	0.000	0.151	0.000
F11	0.164	0.000	0.039	0.038	0.076	0.000	0.407	0.000
F12	0.160	0.000	0.036	0.111	0.048	0.000	0.164	0.000
F13	0.165	0.000	0.038	0.050	0.077	0.000	0.407	0.000

References

1. United Nations General Assembly. *Transforming Our World: The 2030 Agenda for Sustainable Development*; United Nations General Assembly: New York, NY, USA, 2015.
2. FAO. *World Food and Agriculture—Statistical Yearbook 2021*; FAO: Rome, Italy, 2021. <https://doi.org/10.4060/cb4477en>.

3. Zhang, R.; Pei, J.; Zhang, R.; Wang, S.; Zeng, W.; Huang, D.; Wang, Y.; Zhang, Y.; Wang, Y.; Yu, K. Occurrence and distribution of antibiotics in mariculture farms, estuaries and the coast of the Beibu Gulf, China. Bioconcentration and diet safety of seafood. *Ecotoxicol. Environ. Saf.* **2018**, *154*, 27–35. <https://doi.org/10.1016/j.ecoenv.2018.02.006>.
4. FAO. *The State of World Fisheries and Aquaculture 2020 (SOFIA)*; FAO: Rome, Italy, 2020.
5. Alexander, R.B.; Smith, R.A.; Schwarz, G.E. Effect of stream channel size on the delivery of nitrogen to the Gulf of Mexico. *Nature* **2000**, *403*, 758–761. <https://doi.org/10.1038/35001562>.
6. Ps, P.; Aithal, B.H. Building footprint extraction from very high-resolution satellite images using deep learning. *J. Spat. Sci.* **2022**, *10*, 1–17. <https://doi.org/10.1080/14498596.2022.2037473>.
7. Voutsinou-Taliadouri, F. Metal pollution in the Saronikos Gulf. *Mar. Pollut. Bull.* **1981**, *12*, 163–168. [https://doi.org/10.1016/0025-326X\(81\)90228-9](https://doi.org/10.1016/0025-326X(81)90228-9).
8. Ameen, F.; Al-Homaidan, A.A.; Almahasheer, H.; Dawoud, T.; Alwakeel, S.; AlMaarofi, S. Biomonitoring coastal pollution on the Arabian Gulf and the Gulf of Aden using macroalgae. A review. *Mar. Pollut. Bull.* **2022**, *175*, 113156. <https://doi.org/10.1016/j.marpolbul.2021.113156>.
9. DeLaune, R.D.; Wright, A.L. Projected Impact of Deepwater Horizon Oil Spill on U.S. Gulf Coast Wetlands. *Soil Sci. Soc. Am. J.* **2011**, *75*, 1602–1612. <https://doi.org/10.2136/sssaj2011.0168>.
10. Wang, X.; Zhang, Z.; Dai, H. Detection of remote sensing targets with angles via modified CenterNet. *Comput. Electr. Eng.* **2022**, *100*, 107979. <https://doi.org/10.1016/j.compeleceng.2022.107979>.
11. Sahour, H.; Kemink, K.M.; O'Connell, J. Integrating SAR and Optical Remote Sensing for Conservation-Targeted Wetlands Mapping. *Remote Sens.* **2022**, *14*, 159. <https://doi.org/10.3390/rs14010159>.
12. Cui, B.; Fei, D.; Shao, G.; Lu, Y.; Chu, J. Extracting Raft Aquaculture Areas from Remote Sensing Images via an Improved U-Net with a PSE Structure. *Remote Sens.* **2019**, *11*, 2053. <https://doi.org/10.3390/rs11172053>.
13. Wang, Z.; Yang, X.; Liu, Y.; Lu, C. Extraction of coastal raft cultivation area with heterogeneous water background by thresholding object-based visually salient NDVI from high spatial resolution imagery. *Remote Sens. Lett.* **2018**, *9*, 839–846. <https://doi.org/10.1080/2150704X.2018.1468103>.
14. Hu, Y.; Fan, J.; Wang, J. Target recognition of floating raft aquaculture in SAR image based on statistical region merging. In Proceedings of the 2017 Seventh International Conference on Information Science and Technology (ICIST), Da Nang, Vietnam, 16–19 April 2017; pp. 429–432.
15. Duan, Y.; Li, X.; Zhang, L.; Chen, D.; Liu, S.; Ji, H. Mapping national-scale aquaculture ponds based on the Google Earth Engine in the Chinese coastal zone. *Aquaculture* **2020**, *520*, 734666. <https://doi.org/10.1016/j.aquaculture.2019.734666>.
16. Sun, Z.; Luo, J.; Yang, J.; Yu, Q.; Zhang, L.; Xue, K.; Lu, L. Nation-Scale Mapping of Coastal Aquaculture Ponds with Sentinel-1 SAR Data Using Google Earth Engine. *Remote Sens.* **2020**, *12*, 3086. <https://doi.org/10.3390/rs12183086>.
17. Wu, J.; Del Valle, T.M.; Ruckelshaus, M.; He, G.; Fu, Y.; Deng, J.; Liu, J.; Yang, W. Dramatic mariculture expansion and associated driving factors in Southeastern China. *Landsc. Urban Plan.* **2021**, *214*, 104190. <https://doi.org/10.1016/j.landurbplan.2021.104190>.
18. Jia, M.; Wang, Z.; Mao, D.; Ren, C.; Wang, C.; Wang, Y. Rapid, robust, and automated mapping of tidal flats in China using time series Sentinel-2 images and Google Earth Engine. *Remote Sens. Environ.* **2021**, *255*, 112285. <https://doi.org/10.1016/j.rse.2021.112285>.
19. Zhang, K.; Dong, X.; Liu, Z.; Gao, W.; Hu, Z.; Wu, G. Mapping Tidal Flats with Landsat 8 Images and Google Earth Engine. A Case Study of the China's Eastern Coastal Zone circa 2015. *Remote Sens.* **2019**, *11*, 924. <https://doi.org/10.3390/rs11080924>.
20. Li, Q.; Jin, R.; Ye, Z.; Gu, J.; Dan, L.; He, J.; Christakos, G.; Agusti, S.; Duarte, C.M.; Wu, J. Mapping seagrass meadows in coastal China using GEE. *Geocarto Int.* **2022**, *37*, 1–16. <https://doi.org/10.1080/10106049.2022.2070672>.
21. Akhoondzadeh, M. Advances in Seismo-LAI anomalies detection within Google Earth Engine (GEE) cloud platform. *Adv. Space Res.* **2022**, *69*, 4351–4357. <https://doi.org/10.1016/j.asr.2022.03.033>.
22. Yu, Z.; Chang, R.; Chen, Z. Automatic Detection Method for Loess Landslides Based on GEE and an Improved YOLOX Algorithm. *Remote Sens.* **2022**, *14*, 4599. <https://doi.org/10.3390/rs14184599>.
23. Gumma, M.K.; Thenkabail, P.S.; Panjala, P.; Teluguntla, P.; Yamano, T.; Mohammed, I. Multiple agricultural cropland products of South Asia developed using Landsat-8 30 m and MODIS 250 m data using machine learning on the Google Earth Engine (GEE) cloud and spectral matching techniques (SMTs) in support of food and water security. *GIScience Remote Sens.* **2022**, *59*, 1048–1077. <https://doi.org/10.1080/15481603.2022.2088651>.
24. Tamiminia, H.; Salehi, B.; Mahdianpari, M.; Quackenbush, L.; Adeli, S.; Brisco, B. Google Earth Engine for geo-big data applications. A meta-analysis and systematic review. *ISPRS J. Photogramm. Remote Sens.* **2020**, *164*, 152–170. <https://doi.org/10.1016/j.isprsjprs.2020.04.001>.
25. Waleed, M.; Mubeen, M.; Ahmad, A.; Habib-ur-Rahman, M.; Amin, A.; Farid, H.U.; Hussain, S.; Ali, M.; Qaisrani, S.A.; Nasim, W.; et al. Evaluating the efficiency of coarser to finer resolution multispectral satellites in mapping paddy rice fields using GEE implementation. *Sci. Rep.* **2022**, *12*, 13210. <https://doi.org/10.1038/s41598-022-17454-y>.
26. Sha, T.; Yao, X.; Wang, Y.; Tian, Z. A Quick Detection of Lake Area Changes and Hazard Assessment in the Qinghai-Tibet Plateau Based on GEE. A Case Study of Tuosu Lake. *Front. Earth Sci.* **2022**, *10*, 103. <https://doi.org/10.3389/feart.2022.934033>.
27. Cheng, B.; Liang, C.; Liu, X.; Liu, Y.; Ma, X.; Wang, G. Research on a novel extraction method using Deep Learning based on GF-2 images for aquaculture areas. *Int. J. Remote Sens.* **2020**, *41*, 3575–3591. <https://doi.org/10.1080/01431161.2019.1706009>.

28. Kang, J.; Sui, L.; Yang, X.; Liu, Y.; Wang, Z.; Wang, J.; Yang, F.; Liu, B.; Ma, Y. Sea Surface-Visible Aquaculture Spatial-Temporal Distribution Remote Sensing. A Case Study in Liaoning Province, China from 2000 to 2018. *Sustainability* **2019**, *11*, 7186. <https://doi.org/10.3390/su11247186>.
29. Zhang, Y.; Wang, C.; Chen, J.; Wang, F. Shape-Constrained Method of Remote Sensing Monitoring of Marine Raft Aquaculture Areas on Multitemporal Synthetic Sentinel-1 Imagery. *Remote Sens.* **2022**, *14*, 1249. <https://doi.org/10.3390/rs14051249>.
30. Duan, Y.; Li, X.; Zhang, L.; Liu, W.; Liu, S.; Chen, D.; Ji, H. Detecting spatiotemporal changes of large-scale aquaculture ponds regions over 1988–2018 in Jiangsu Province, China using Google Earth Engine. *Ocean Coast. Manag.* **2020**, *188*, 105144. <https://doi.org/10.1016/j.ocecoaman.2020.105144>.
31. Xu, Y.; Hu, Z.; Zhang, Y.; Wang, J.; Yin, Y.; Wu, G. Mapping Aquaculture Areas with Multi-Source Spectral and Texture Features. A Case Study in the Pearl River Basin (Guangdong), China. *Remote Sens.* **2021**, *13*, 4320. <https://doi.org/10.3390/rs13214320>.
32. Cheng, M.; Jiao, X.; Shi, L.; Penuelas, J.; Kumar, L.; Nie, C.; Wu, T.; Liu, K.; Wu, W.; Jin, X. High-resolution crop yield and water productivity dataset generated using random forest and remote sensing. *Sci. Data* **2022**, *9*, 641. <https://doi.org/10.1038/s41597-022-01761-0>.
33. Loozen, Y.; Rebel, K.T.; de Jong, S.M.; Lu, M.; Ollinger, S.V.; Wassen, M.J.; Karssenbergh, D. Mapping canopy nitrogen in European forests using remote sensing and environmental variables with the random forests method. *Remote Sens. Environ.* **2020**, *247*, 111933. <https://doi.org/10.1016/j.rse.2020.111933>.
34. Wang, Q.; Zhao, L.; Wang, M.; Wu, J.; Zhou, W.; Zhang, Q.; Deng, M. A Random Forest Model for Drought. Monitoring and Validation for Grassland Drought Based on Multi-Source Remote Sensing Data. *Remote Sens.* **2022**, *14*, 4981. <https://doi.org/10.3390/rs14194981>.
35. Ghorbanian, A.; Zaghian, S.; Asiyabi, R.M.; Amani, M.; Mohammadzadeh, A.; Jamali, S. Mangrove Ecosystem Mapping Using Sentinel-1 and Sentinel-2 Satellite Images and Random Forest Algorithm in Google Earth Engine. *Remote Sens.* **2021**, *13*, 2565. <https://doi.org/10.3390/rs13132565>.
36. Matarira, D.; Mutanga, O.; Naidu, M. Google Earth Engine for Informal Settlement Mapping. A Random Forest Classification Using Spectral and Textural Information. *Remote Sens.* **2022**, *14*, 5130. <https://doi.org/10.3390/rs14205130>.
37. Phan, T.N.; Kuch, V.; Lehnert, L.W. Land Cover Classification using Google Earth Engine and Random Forest Classifier—The Role of Image Composition. *Remote Sens.* **2020**, *12*, 2411. <https://doi.org/10.3390/rs12152411>.
38. Ying, Z.; Wu, J.; Del Valle, T.M.; Yang, W. Spatiotemporal dynamics of coastal aquaculture and driving force analysis in South-eastern China. *Ecosyst. Health Sustain.* **2020**, *6*, 1851145. <https://doi.org/10.1080/20964129.2020.1851145>.
39. Giri, S.; Daw, T.M.; Hazra, S.; Troell, M.; Samanta, S.; Basu, O.; Marcinko, C.L.J.; Chanda, A. Economic incentives drive the conversion of agriculture to aquaculture in the Indian Sundarbans: Livelihood and environmental implications of different aquaculture types. *AMBIO* **2022**, *51*, 1963–1977. <https://doi.org/10.1007/s13280-022-01720-4>.
40. Wang, J.-F.; Zhang, T.-L.; Fu, B.-J. A measure of spatial stratified heterogeneity. *Ecol. Indic.* **2016**, *67*, 250–256. <https://doi.org/10.1016/j.ecolind.2016.02.052>.
41. Wang, J.-F.; Li, X.-H.; Christakos, G.; Liao, Y.-L.; Zhang, T.; Gu, X.; Zheng, X.-Y. Geographical Detectors-Based Health Risk Assessment and its Application in the Neural Tube Defects Study of the Heshun Region, China. *Int. J. Geogr. Inf. Sci.* **2010**, *24*, 107–127. <https://doi.org/10.1080/13658810802443457>.
42. Qiao, Y.; Wang, X.; Han, Z.; Tian, M.; Wang, Q.; Wu, H.; Liu, F. Geodetector based identification of influencing factors on spatial distribution patterns of heavy metals in soil. A case in the upper reaches of the Yangtze River, China. *Appl. Geochem.* **2022**, *146*, 105459. <https://doi.org/10.1016/j.apgeochem.2022.105459>.
43. Zhao, R.; Zhan, L.; Yao, M.; Yang, L. A geographically weighted regression model augmented by Geodetector analysis and principal component analysis for the spatial distribution of PM2.5. *Sustain. Cities Soc.* **2020**, *56*, 102106. <https://doi.org/10.1016/j.scs.2020.102106>.
44. Yang, Y.; Yang, X.; He, M.; Christakos, G. Beyond mere pollution source identification. Determination of land covers emitting soil heavy metals by combining PCA/APCS, GeoDetector and GIS analysis. *CATENA* **2020**, *185*, 104297. <https://doi.org/10.1016/j.catena.2019.104297>.
45. Zhou, X.; Wen, H.; Zhang, Y.; Xu, J.; Zhang, W. Landslide susceptibility mapping using hybrid random forest with GeoDetector and RFE for factor optimization. *Geosci. Front.* **2021**, *12*, 101211. <https://doi.org/10.1016/j.gsf.2021.101211>.
46. Gu, J.; Liang, L.; Song, H.; Kong, Y.; Ma, R.; Hou, Y.; Zhao, J.; Liu, J.; He, N.; Zhang, Y. A method for hand-foot-mouth disease prediction using GeoDetector and LSTM model in Guangxi, China. *Sci. Rep.* **2019**, *9*, 17928. <https://doi.org/10.1038/s41598-019-54495-2>.
47. Su, Y.; Li, T.; Cheng, S.; Wang, X. Spatial distribution exploration and driving factor identification for soil salinisation based on geodetector models in coastal area. *Ecol. Eng.* **2020**, *156*, 105961. <https://doi.org/10.1016/j.ecoleng.2020.105961>.
48. Yuanxin, Y. Lethal effects of suspended sediment on juvenile and young *Acanthopagrus latus* in Bachimen waters of Dongshan. *J. Fish. Res.* **2021**, *43*, 571–577.
49. Xiang, L. Principal Component Linear Regression Analysis on Chlorophyll-a and Environmental Factors in Aquiculture Area, Zhao'an Bay. *Environ. Impact Assess.* **2018**, *40*, 88–96.
50. Yingyu, X.; Jiao, L.; Yongqing, L.; Miaofeng, Y. Distributional and risk assessment of Hg and As in the culture-shellfish from southern coastal areas of Fujian Province. *Environ. Chem.* **2017**, *36*, 1009–1016.

51. Shuoliang, Z.; Jingshan, R.; Yingyu, X.; Lifeng, W.; Shenghua, Z.; Miaofeng, Y.; Ying, Y.; Yufeng, C. Study on assessment and categorization for the eco—Environmental quality of shellfish—Culture regions in Zhao'an Bay, Fujian province. *J. Fujian Fish.* **2012**, *34*, 268–276.
52. Ministry of Natural Resources, PRC. Bulletin on China's Marine Ecological Environment in 2021. 2022. Available online: http://news.mnr.gov.cn/dt/hy/202206/t20220606_2738442.html (accessed on 6 Jun 2022).
53. Arcgis Pro. 2019. Retrieved from <https://www.esri.com/zh-cn/arcgis/products/arcgis-pro/overview> (accessed on 3 May 2019).
54. Ruff, E.O.; Gentry, R.R.; Clavelle, T.; Thomas, L.R.; Lester, S.E. Governance and mariculture in the Caribbean. *Mar. Policy* **2019**, *107*, 103565. <https://doi.org/10.1016/j.marpol.2019.103565>.
55. Sarker, S.; Akter, M.; Rahman, M.S.; Islam, M.M.; Hasan, O.; Kabir, M.A.; Rahman, M.M. Spatial prediction of seaweed habitat for mariculture in the coastal area of Bangladesh using a Generalized Additive Model. *Algal Res.* **2021**, *60*, 102490. <https://doi.org/10.1016/j.algal.2021.102490>.
56. Sánchez-Jerez, P.; Babarro, J.M.; Padin, X.A.; Portabales, A.L.; Martínez-Llorens, S.; Ballester-Berman, J.D.; Sara, G.; Mangano, M.C. Cumulative climatic stressors strangles marine aquaculture. Ancillary effects of COVID 19 on Spanish mariculture. *Aquaculture* **2022**, *549*, 737749. <https://doi.org/10.1016/j.aquaculture.2021.737749>.
57. Hillger, D.; Seaman, C.; Liang, C.; Miller, S.; Lindsey, D.; Kopp, T. Suomi NPP VIIRS Imagery evaluation. *J. Geophys. Res. Atmos.* **2014**, *119*, 6440–6455. <https://doi.org/10.1002/2013JD021170>.
58. Gashaw, T.; Tulu, T.; Argaw, M.; Worqlul, A.W.; Tolessa, T.; Kindu, M. Estimating the impacts of land use/land cover changes on Ecosystem Service Values. The case of the Andassa watershed in the Upper Blue Nile basin of Ethiopia. *Ecosyst. Serv.* **2018**, *31*, 219–228. <https://doi.org/10.1016/j.ecoser.2018.05.001>.
59. Van Asselen, S.; Verburg, P.H.; Vermaat, J.E.; Janse, J.H. Drivers of wetland conversion. A global meta-analysis. *PLoS ONE* **2013**, *8*, e81292. <https://doi.org/10.1371/journal.pone.0081292>.
60. Wang, L.; Yue, X.; Wang, H.; Ling, K.; Liu, Y.; Wang, J.; Hong, J.; Pen, W.; Song, H. Dynamic Inversion of Inland Aquaculture Water Quality Based on UAVs-WSN Spectral Analysis. *Remote Sens.* **2020**, *12*, 402. <https://doi.org/10.3390/rs12030402>.
61. Song, C.; Becagli, S.; Beddows, D.C.S.; Brean, J.; Browse, J.; Dai, Q.; Dall'Osto, M.; Ferracci, V.; Harrison, R.M.; Harris, N.; et al. Understanding Sources and Drivers of Size-Resolved Aerosol in the High Arctic Islands of Svalbard Using a Receptor Model Coupled with Machine Learning. *Environ. Sci. Technol.* **2022**, *56*, 11189–11198. <https://doi.org/10.1021/acs.est.1c07796>.
62. Chopin, T.; Cooper, J.A.; Reid, G.; Cross, S.; Moore, C. Open-water integrated multi-trophic aquaculture. Environmental bio-mitigation and economic diversification of fed aquaculture by extractive aquaculture. *Rev. Aquac.* **2012**, *4*, 209–220. <https://doi.org/10.1111/j.1753-5131.2012.01074.x>.
63. Ren, C.; Wang, Z.; Zhang, Y.; Zhang, B.; Chen, L.; Xi, Y.; Xiao, X.; Doughty, R.B.; Liu, M.; Jia, M.; et al. Rapid expansion of coastal aquaculture ponds in China from Landsat observations during 1984–2016. *Int. J. Appl. Earth Obs. Geoinf.* **2019**, *82*, 101902. <https://doi.org/10.1016/j.jag.2019.101902>.
64. Liu, S. Effect of reclamation activities on wetlands in Estuarine Delta in China. *Wetl. Sci.* **2013**, *11*, 297–304.
65. Chen, H.; Zhao, Y.; Fu, X.; Tang, M.; Guo, M.; Zhang, S.; Zhu, Y.; Qu, L.; Wu, G. Impacts of regional land-use patterns on ecosystem services in the typical agro-pastoral ecotone of northern China. *Ecosyst. Health Sustain.* **2022**, *8*, 2110521. <https://doi.org/10.1080/20964129.2022.2110521>.
66. Foley, J.A.; DeFries, R.; Asner, G.P.; Barford, C.; Bonan, G.; Carpenter, S.R.; Chapin, F.S.; Coe, M.T.; Daily, G.C.; Gibbs, H.K.; et al. Global Consequences of Land Use. *Science* **2005**, *309*, 570–574. <https://doi.org/10.1126/science.1111772>.
67. Ministry of Natural Resources, PRC. Bulletin on China's Marine Ecological Environment in 2019. 2020. Available online: <https://www.mee.gov.cn/hjzl/sthjzk/jagb/202006/P020200603371117871012.pdf> (accessed on 1 Jun 2020).
68. Zhao'an County People's Government Office. Notice of Zhao'an County People's Government Office on Printing and Distributing the Work Plan of Zhao'an County on the Control of Fishery Pollution Sources. 2019. Retrieved from <http://www.zhaoan.gov.cn/cms/html/zaxnzz/2019-11-08/1359531076.html> (accessed on 8 Nov 2019).
69. Zhao'an County Bureau of Ocean and Fisheries. A Reply Letter on the Handling of the 4th Session of the 17th County People's Congress No. 39 Representative's Proposal. 2020. Available online: <http://search.zhangzhou.gov.cn/cms/infopublic/publicInfo.shtml?id=60502325480150004> (accessed on 6 Jul 2020).
70. Sun, X.; Zhang, L.; Lu, S.-Y.; Tan, X.-Y.; Chen, K.-L.; Zhao, S.-Q.; Huang, R.-H. A new model for evaluating sustainable utilization of coastline integrating economic output and ecological impact. A case study of coastal areas in Beibu Gulf, China. *J. Clean. Prod.* **2020**, *271*, 122423. <https://doi.org/10.1016/j.jclepro.2020.122423>.
71. Zhou, Y.; Li, X.; Liu, Y. Land use change and driving factors in rural China during the period 1995–2015. *Land Use Policy* **2020**, *99*, 105048. <https://doi.org/10.1016/j.landusepol.2020.105048>.
72. Liu, L. Current situation and countermeasures of sea reclamation in China. *Guangzhou Environ. Sci.* **2008**, *2*, 26–30.
73. Wang, W.; Liu, H.; Li, Y.; Su, J. Development and management of land reclamation in China. *Ocean Coast. Manag.* **2014**, *102*, 415–425. <https://doi.org/10.1016/j.ocecoaman.2014.03.009>.
74. Wang, X.; Zhou, T.; Ying, Z.; Jing, W.U.; Yang, W. Analyses of water quality and driving forces in Ningde aquaculture area. *Acta Ecol. Sin.* **2020**, *40*, 1766–1778.

75. Ren, C.; Wang, Z.; Zhang, B.; Li, L.; Chen, L.; Song, K.; Jia, M. Remote Monitoring of Expansion of Aquaculture Ponds Along Coastal Region of the Yellow River Delta from 1983 to 2015. *Chin. Geogr. Sci.* **2018**, *28*, 430–442. <https://doi.org/10.1007/s11769-017-0926-2>.
76. MacKinnon, J.; Verkuil, Y.; Murray, N. *IUCN Situation Analysis on East and Southeast Asian Intertidal Habitats, with Particular Reference to the Yellow Sea (including the Bohai Sea)*; IUCN: Gland, Switzerland, 2012; p. 47. Available online: <https://portals.iucn.org/library/efiles/documents/SSC-OP-047.pdf> (accessed on 1 Jan 2012).
77. Morgera, E.; Vrancken, P. The ocean, sustainable development and human rights. *RECIEL* **2022**, *31*, 333–335. <https://doi.org/10.1111/reel.12480>.
78. Nash, K.L.; van Putten, I.; Alexander, K.A.; Bettiol, S.; Cvitanovic, C.; Farmery, A.K.; Flies, E.J.; Ison, S.; Kelly, R.; Mackay, M.; et al. Oceans and society. Feedbacks between ocean and human health. *Rev. Fish Biol. Fish.* **2022**, *32*, 161–187. <https://doi.org/10.1007/s11160-021-09669-5>.
79. Grant, S.M.; Waller, C.L.; Morley, S.A.; Barnes, D.K.A.; Brasier, M.J.; Double, M.C.; Griffiths, H.J.; Hughes, K.A.; Jackson, J.A.; Waluda, C.M.; et al. Local Drivers of Change in Southern Ocean Ecosystems. Human Activities and Policy Implications. *Front. Ecol. Evol.* **2021**, *9*, 624518. <https://doi.org/10.3389/fevo.2021.624518>.
80. Pellens, N.; Boelee, E.; Veiga, J.M.; Fleming, L.E.; Blauw, A. Innovative actions in oceans and human health for Europe. *Health Promot. Int.* **2021**, *2021*, daab203. <https://doi.org/10.1093/heapro/daab203>.
81. Hair, C.; Foale, S.; Daniels, N.; Minimulu, P.; Aini, J.; Southgate, P.C. Social and economic challenges to community-based sea cucumber mariculture development in New Ireland Province, Papua New Guinea. *Mar. Policy* **2020**, *117*, 103940. <https://doi.org/10.1016/j.marpol.2020.103940>.
82. La Aslan, O.M.; Iba, W.; La Bolu, O.R.; Ingram, B.A.; Gooley, G.J.; de Silva, S.S. Mariculture in SE Sulawesi, Indonesia. Culture practices and the socio economic aspects of the major commodities. *Ocean Coast. Manag.* **2015**, *116*, 44–57. <https://doi.org/10.1016/j.ocecoaman.2015.06.028>.
83. Rodrigues, J.M.F.; Cardoso, P.J.S.; Monteiro, J.; Lam, R.; Krzhizhanovskaya, V.V.; Lees, M.H.; Dongarra, J.J.; Sloot, P.M.; Lou, Y.; Chen, L.; et al. (Eds.) *Research and Implementation of an Aquaculture Monitoring System Based on Flink, MongoDB and Kafka. Computational Science—ICCS 2019*; Springer International Publishing: Berlin/Heidelberg, Germany, 2019.
84. Ubina, N.A.; Cheng, S.-C. A Review of Unmanned System Technologies with Its Application to Aquaculture Farm Monitoring and Management. *Drones* **2022**, *6*, 12. <https://doi.org/10.3390/drones6010012>.
85. Alwis, S.D.; Hou, Z.; Zhang, Y.; Na, M.H.; Ofoghi, B.; Sajjanhar, A. A survey on smart farming data, applications and techniques. *Comput. Ind.* **2022**, *138*, 103624. <https://doi.org/10.1016/j.compind.2022.103624>.
86. Kirankumar, P.; Keertana, G.; Sivarao, S.U.A.; Vijaykumar, B.; Shah, S.C. Smart Monitoring and Water Quality Management in Aquaculture using IOT and ML. In Proceedings of the 2021 IEEE International Conference on Intelligent Systems, Smart and Green Technologies (ICISSGT), Visakhapatnam, India, 13–14 Nov. 2021. <https://doi.org/10.1109/ICISSGT52025.2021.00018>.
87. Zhao, S.; Zhang, S.; Liu, J.; Wang, H.; Zhu, J.; Li, D.; Zhao, R. Application of machine learning in intelligent fish aquaculture. A review. *Aquaculture* **2021**, *540*, 736724. <https://doi.org/10.1016/j.aquaculture.2021.736724>.
88. Craig, R.K. Fostering Adaptive Marine Aquaculture through Procedural Innovation in Marine Spatial Planning. *Marine Policy*, **2019**, *110*, 103555.
89. Douvère, F.; Ehler, C.N. New perspectives on sea use management. Initial findings from European experience with marine spatial planning. *J. Environ. Manag.* **2009**, *90*, 77–88. <https://doi.org/10.1016/j.jenvman.2008.07.004>.
90. Yu, J.-K.; Li, Y.-H. Evolution of marine spatial planning policies for mariculture in China. Overview, experience and prospects. *Ocean Coast. Manag.* **2020**, *196*, 105293. <https://doi.org/10.1016/j.ocecoaman.2020.105293>.
91. Filgueira, R.; Grant, J.; Strand, Ø. Implementation of marine spatial planning in shellfish aquaculture management. Modeling studies in a Norwegian fjord. *Ecol. Appl.* **2014**, *24*, 832–843. <https://doi.org/10.1890/13-0479.1>.
92. Roth, E.; Burbridge, P.; Hendrick, V.; Rosenthal, H. Social and economic policy issues relevant to marine aquaculture. *J. Appl. Ichthyol.* **2001**, *17*, 194–206. <https://doi.org/10.1046/j.1439-0426.2001.00316.x>.

Disclaimer/Publisher’s Note: The statements, opinions and data contained in all publications are solely those of the individual author(s) and contributor(s) and not of MDPI and/or the editor(s). MDPI and/or the editor(s) disclaim responsibility for any injury to people or property resulting from any ideas, methods, instructions or products referred to in the content.